© 2015. Published by The Company of Biologists Ltd | Journal of Cell Science (2015) 128, 1887-1900 doi:10.1242/jcs.148296

RESEARCH ARTICLE

PML induces compaction, TRF2 depletion and DNA damage signaling at telomeres and promotes their alternative lengthening

Sarah Osterwald[1,§], Katharina I. Deeg[1,§], Inn Chung[1,*], Daniel Parisotto[1,‡], Stefan Wörz[2], Karl Rohr[2], Holger Erfle[3] and Karsten Rippe[1,¶]

ABSTRACT

The alternative lengthening of telomeres (ALT) mechanism allows cancer cells to escape senescence and apoptosis in the absence of active telomerase. A characteristic feature of this pathway is the assembly of ALT-associated promyelocytic leukemia (PML) nuclear bodies (APBs) at telomeres. Here, we dissected the role of APBs in a human ALT cell line by performing an RNA interference screen using an automated 3D fluorescence microscopy platform and advanced 3D image analysis. We identified 29 proteins that affected APB formation, which included proteins involved in telomere and chromatin organization, protein sumoylation and DNA repair. By integrating and extending these findings, we found that APB formation induced clustering of telomere repeats, telomere compaction and concomitant depletion of the shelterin protein TRF2 (also known as TERF2). These APB-dependent changes correlated with the induction of a DNA damage response at telomeres in APBs as evident by a strong enrichment of the phosphorylated form of the ataxia telangiectasia mutated (ATM) kinase. Accordingly, we propose that APBs promote telomere maintenance by inducing a DNA damage response in ALT-positive tumor cells through changing the telomeric chromatin state to trigger ATM phosphorylation.

KEY WORDS: Alternative lengthening of telomeres, ALT, ALT-associated PML nuclear body, APB, DNA repair, PML nuclear bodies

INTRODUCTION

The gradual shortening of telomeres during replication eventually triggers growth arrest and senescence and thus provides an important tumor suppressor mechanism (d'Adda di Fagagna et al., 2003; Harley et al., 1990). Cancer cells overcome this proliferation limit by activating a telomere maintenance mechanism. In most cases telomerase is re-activated, which can extend the telomere repeat sequence TTAGGG (Shay and Bacchetti, 1997). However, 10–15% of tumors employ an alternative lengthening of telomeres (ALT) mechanism to elongate their chromosomal ends by DNA recombination and repair processes in the absence of telomerase (Bryan et al., 1997). ALT tumors are typically characterized by a large heterogeneity in telomere length within one cell (Bryan et al., 1995), the occurrence of extrachromosomal telomeric repeats (ECTRs) (Wang et al., 2004), mutations of the chromatin remodeler ATRX (Heaphy et al., 2011), genome instability (Lovejoy et al., 2012), increased telomeric recombination (Londoño-Vallejo et al., 2004) and the presence of ALT-associated promyelocytic leukemia (PML) nuclear bodies (APBs) (Chung et al., 2012; Yeager et al., 1999). APBs are defined as complexes of PML nuclear bodies (PML-NBs) with telomeric DNA in telomerase-negative cells (Yeager et al., 1999), and their ectopic assembly in ALT-positive cells induces telomere lengthening by promoting repair-associated DNA synthesis (Chung et al., 2011). A number of proteins involved in ALT have been identified, such as the telomeric shelterin complex (Jiang et al., 2007), the small ubiquitin-like modifier (SUMO) E3 ligase MMS21 (also known as NSMCE2) (Potts and Yu, 2007), several DNA repair proteins (Nabetani and Ishikawa, 2011), as well as heterochromatin protein 1 (HP1) family proteins (Jiang et al., 2009). However, the molecular details of the ALT pathway have remained elusive.

Here, we applied a three-dimensional (3D) confocal laser scanning microscopy (CLSM) screening platform and quantitative image analysis to evaluate changes in the nuclear organization of APBs, PML-NBs and telomeres at high precision based on the analysis of more than 20 million images. With this approach, we were able to characterize features of single telomeres in their native cellular context and compare the effect of small interfering RNA (siRNA)-mediated knockdown of ∼100 genes by analyzing a comprehensive set of image-based readouts. Our results reveal that depletion of APBs by long-term PML knockdown leads to telomere shortening and a reduction of ECTRs. In addition, we found that PML induced clustering and compaction of colocalizing telomere repeats and, simultaneously, reduced binding of the telomeric repeat binding factor 2 (TRF2, also known as TERF2). These changes in telomere organization correlated with the activation of the ataxia telangiectasia mutated (ATM) kinase in APBs. Based on these findings, we propose a model for APB-mediated telomere lengthening in ALT-positive cells and tumors.

RESULTS

PML knockdown induces telomere shortening and reduces ECTRs

PML is the central structural component for forming PML-NBs and APBs. In the absence of PML, other PML-NB components, such as SP100 and SUMO, do not assemble into a nuclear subcompartment (Ishov et al., 1999; Tavalai et al., 2006; Zhong et al., 2000). Accordingly, we investigated the role of PML protein in ALT by using an ALT-positive human U2OS osteosarcoma cell line with an inducible stable knockdown of PML that targets a sequence common to the seven PML isoforms. Immunofluorescence analysis using a pan PML antibody that detects all isoforms was conducted

[1]Research Group Genome Organization & Function, Deutsches Krebsforschungszentrum (DKFZ) & BioQuant, 69120 Heidelberg, Germany. [2]Department of Bioinformatics and Functional Genomics, Biomedical Computer Vision Group, University of Heidelberg & DKFZ, BioQuant, IPMB, 69120 Heidelberg, Germany. [3]ViroQuant-CellNetworks RNAi Screening Facility, University of Heidelberg & BioQuant, 69120 Heidelberg, Germany.
*Present address: Molecular Biology Program, Memorial Sloan-Kettering Cancer Center, New York, NY 10065, USA. ‡Present address: Department of Biochemistry, Weill Cornell Medical College, New York, NY 10065, USA.
§These authors contributed equally to this work

¶Author for correspondence (Karsten.Rippe@dkfz.de)

Received 27 August 2014; Accepted 23 March 2015

Journal of Cell Science (2015) 128, 1887-1900 doi:10.1242/jcs.148296

and evaluated with our previously developed quantitative automated 3D confocal image acquisition and analysis platform (Osterwald et al., 2012; Wörz et al., 2010) (supplementary material Fig. S1). The results showed that the number of PML-NBs was reduced by 99.3±0.1% (mean±s.e.m.) after 72 h of PML knockdown (P<0.001, Fig. 1A). The knockdown completely suppressed colocalizations between PML and telomeres and thus APB formation (–3.5±0.3 APBs per cell and –99.7±0.3%, respectively, P<0.001, Table 1). The disappearance of APBs was accompanied by a reduction in the amount of C-circles, which are ALT-specific partially single-stranded telomeric $(CCCTAA)_n$ DNA circles (–87.5±4.1%, P<0.001, Fig. 1C). At the same time, the number of detectable telomere repeat foci per cell was significantly increased (+6.5±2.6, P<0.001, Table 1). The reduced fluorescence intensities of the Cy3-labeled telomere repeats after 72 h revealed that high-intensity telomere repeat signals disintegrated into several low-intensity telomere repeat foci (median, –12.8±2.0%, P<0.001, Fig. 1D). Thus, on average, the number of detectable telomere repeat foci increased upon PML knockdown by one to two for every APB that disappeared, indicating telomere clustering in APBs.

To assess whether PML is needed for telomere elongation in ALT cells, we performed a long-term PML knockdown in U2OS cells for 30 days, which corresponds to approximately 30 population doublings. The knockdown led to a significant decrease of the telomere repeat signal intensity (median, –24.9±1.7%, P<0.001, Fig. 1B,D) as detected by interphase quantitative fluorescence *in situ* hybridization (Q-FISH), which was more pronounced than the short-term effect observed after 72 h of knockdown. This reduction of telomere content upon long-term PML knockdown was confirmed by telomere-repeat quantitative PCR (supplementary material Fig. S2A). In addition, terminal restriction fragment (TRF) analysis after 2, 4 and 6 weeks of PML knockdown revealed that PML knockdown induced telomere shortening (supplementary material Fig. S2B). Next, we performed Q-FISH on metaphase chromosomes of uninduced and induced PML knockdown cells (Fig. 1E; Table 2). This method is well established to detect and quantify ECTRs and has been used in a number of previous studies (Episkopou et al., 2014; Hande et al., 2001; Kamranvar et al., 2013; Kamranvar and Masucci, 2011; Tokutake et al., 1998). Note that we refer here to those ECTRs that are detected by a peptide nucleic acid (PNA) FISH probe against the G-rich telomere repeat sequence. This group of ECTRs is distinct from the single-stranded C-rich C-circles measured by rolling circle amplification according to the method of Henson et al. (Henson et al., 2009), which would not give rise to a signal in our telomere-repeat FISH assay. The intensity of telomere repeats associated with chromosomes was significantly reduced after 30 days of PML knockdown (median, –18.6±9.6%, P<0.001, Table 2), and considerably more telomere-free ends were detected (52.5±26.5%, P<0.05, Table 2). The number of detectable ECTRs – defined as telomere repeat signals per metaphase spread that were not associated with chromosomes – was reduced by 59.8±10.2% (P<0.001, Table 2). In general, ECTRs had a lower median repeat intensity than the telomeres. They accounted for only ∼7% of the total telomere repeat intensity per metaphase spread in uninduced control cells, thus representing a small fraction of the total telomere repeat signal (Table 2). This finding agrees well with a recent study that also quantified the contribution of ECTRs to total telomere repeat content in ALT cells by performing both Q-FISH and extraction of extrachromosomal DNA and subsequent Southern blotting (Episkopou et al., 2014). Accordingly, we conclude that the telomere repeat signal measured in interphase FISH experiments (Table 2) mainly originates from telomeres and only a small fraction represents ECTRs.

In summary, interphase and metaphase Q-FISH, TRF analysis and telomere quantitative PCR consistently reveal that telomere shortening is induced upon PML knockdown that is accompanied by a reduction of ECTRs, including both C-circles and G-rich ECTRs.

An RNAi screen with automated 3D image analysis identifies 29 proteins involved in APB formation

Having shown that depletion of APBs by PML knockdown led to telomere shortening, we set out to identify factors that disrupt PML assembly into APBs and thus could affect the ALT pathway. We conducted an RNA interference (RNAi) screen by quantitative automated 3D confocal imaging and subsequent analysis of telomere, PML-NB and APB features, as described in further detail previously (Osterwald et al., 2012; Wörz et al., 2010). Briefly, ∼100 candidate proteins were knocked down by two independent small interfering RNAs (siRNAs) (supplementary material Table S1). Then the number, volume, intensity and density (defined as intensity per volume) of telomere repeats and PML-NBs, and their colocalization, representing APBs, were determined from the automated analysis of more than 20 million images (supplementary material Fig. S1). In this manner, we were able to reliably quantify changes in APB formation and telomere organization at the level of single telomeres with high precision in order to dissect the function of APBs.

From our RNAi screen, we identified 29 proteins involved in APB formation (supplementary material Table S2). Only those proteins that showed a significant change of more than 10% in the number of APBs (P<0.05) for two different siRNAs in at least three independent experiments were selected as hits. Other ‘non-hit’ proteins that did not meet these relatively strict requirements were classified into two groups (supplementary material Table S2): (1) targets where both siRNAs consistently did not show a significant effect on the number of APBs, considered as proteins that do not have an effect on APB formation; and (2) targets where only one out of two siRNAs showed a significant effect, representing candidates that could have an effect on APB formation. However, these were not further investigated here. The knockdown efficiency of selected hits as well as non-hits was analyzed by quantitative real-time PCR (supplementary material Fig. S3A) unless already previously validated (supplementary material Table S1). Based on the associated biological processes according to gene ontology (GO) annotation, the APB effector proteins were grouped into proteins involved in telomere organization, protein sumoylation, DNA repair and chromatin organization (Table 3).

As inferred from our previous work, the number of APBs displayed little dependence on cell cycle state in normally proliferating U2OS cells (Osterwald et al., 2012), although the number of PML-NBs was higher during S-phase in this cell line (Dellaire et al., 2006). For other cell lines, a higher number of APBs has been reported after inducing a cell cycle arrest in G2/M phase for human ovarian surface epithelium (HOSE) cells (Grobelny et al., 2000) or in G0/G1 phase for IIICF/c and GM847 cell lines (Jiang et al., 2007). Accordingly, we addressed the question of whether the siRNA knockdowns conducted here were associated with significant changes in the proportion of cells in each phase of the cell cycle. The integrated background-corrected DAPI intensities per cell nucleus were computed for a given sample from the confocal image stacks and used to obtain the relative cellular DNA content as described previously (Tóth et al., 2004; Osterwald et al., 2012). From this quantification the cell cycle distribution was determined by applying an identical predefined gating of the DNA content histograms for G1, S and G2/M phase and

Journal of Cell Science (2015) 128, 1887-1900 doi:10.1242/jcs.148296

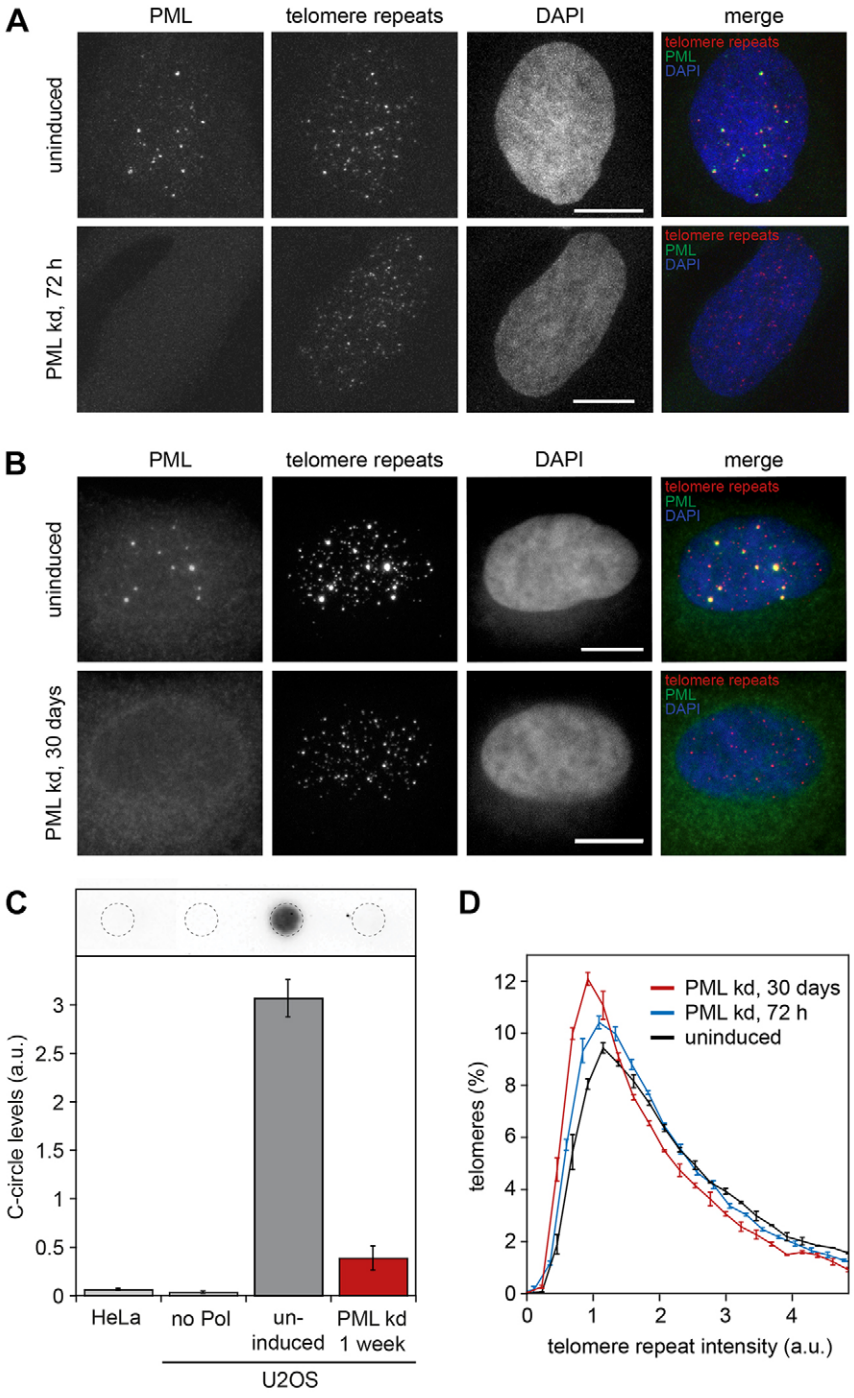

Fig. 1. PML knockdown induces loss of telomere repeats and reduces ECTRs. The effect of an inducible PML knockdown on ALT features was evaluated at different time points in comparison to uninduced U2OS cells. (A,B) CLSM images of uninduced and induced cells after 72 h (A) and 30 days (B) of PML knockdown (kd), stained by FISH with a Cy3-labeled telomere repeat probe and by immunofluorescence against PML. Images of uninduced and induced cells were acquired with identical microscope settings. Scale bars: 10 µm. (C) C-circle levels in uninduced and induced PML knockdown U2OS cells after 1 week of induction. As control, ALT-negative HeLa cells and uninduced PML knockdown U2OS cells without addition of polymerase (no Pol) were used. Results represent mean±s.e.m. (n=6). (D) Relative frequency distributions of the fluorescence intensity of the Cy3-labeled telomere repeat probe measured at individual telomeres in uninduced cells and after PML knockdown for 72 h and 30 days, respectively. The difference in telomere repeat intensity after 72 h and 30 days of PML knockdown in comparison to uninduced cells is statistically significant (P<0.001, Kolmogorov–Smirnov test). At least 20,000 telomeres were analyzed for each experiment. (E) Metaphase spreads of uninduced and induced PML knockdown U2OS cells after 30 days of induction. Telomeres were visualized using telomeric FISH probes. Asterisks indicate ECTRs and arrowheads telomere-free ends. Images were acquired with identical microscope settings. Scale bars: 10 µm.

Journal of Cell Science (2015) 128, 1887-1900 doi:10.1242/jcs.148296

Table 1. ALT features after PML knockdown for 72 h

	APBs per cell	Telomere repeat foci per cell	Telomere repeat density (a.u.)	Telomere volume (10^{-3} μm^3)	TRF2 signal to telomere repeat signal ratio
Uninduced	3.5±0.3	62.6±3.1	15.9±0.3	12.5±0.1	0.65±0.01
Induced PML knockdown	0.01±0.01	69.1±1.8	14.3±0.4	11.8±0.1	0.91±0.01
Difference between induced and uninduced	–3.5±0.3	6.5±2.6	–1.6±0.6	–0.7±0.1	0.26±0.01
Difference between induced and uninduced (%)	–99.7±0.3**	10.8±4.6**	–9.9±3.4**	–5.5±1.1**	41.9±8.2**

The telomere repeat density is the integrated signal intensity of a telomere labeled by FISH divided by the volume of that telomere. The TRF2 signal to telomere repeat signal ratio is the density of the TRF2 immunofluorescence signal divided by the telomere repeat density of the colocalizing telomere FISH signal. Results are mean±s.e.m. (n>1000 cells per treatment). **P<0.001 (Kolmogorov–Smirnov test).

computing the corresponding percentage of cells within each group (supplementary material Fig. S3B). For the majority of knockdown experiments no significant change in the proportion of cells in each phase of the cell cycle was observed under our experimental conditions (supplementary material Table S2). For six targets (BLM, CDKN1A, FEN1, LSD1, MORC3 and UBC9) a significant change, in the range of 10 percentage points for cells in G1 or G2/M, but not in S phase, was observed for one of the siRNAs in comparison to control siRNA. However, the direction of the measured change in the number of APBs for siRNAs targeting FEN1, UBC9 and CDKN1A did not correspond to that observed previously in cell cycle arrest experiments with IIICF/c, GM847 or HOSE cells (Grobelny et al., 2000; Jiang et al., 2007). Thus, we conclude that in general the changes in the number of PML-NBs and APBs measured here for the U2OS cell line upon siRNA-mediated protein knockdown were not due to changes in the cell cycle distribution.

Changes in chromatin compaction affect TRF2 binding to telomere repeats, APB formation and C-circle levels

Next, we evaluated the link between telomeric chromatin organization and APB formation. Interestingly, knockdown of several factors involved in heterochromatin formation, for example, the histone methyltransferase SUV4-20H2 (Benetti et al., 2007; Schotta et al., 2004), heterochromatin protein 1γ (HP1γ, also known as CBX3) (Jiang et al., 2011; Jiang et al., 2009; Verschure et al., 2005) or the histone demethylase LSD1 (Shi et al., 2004), reduced the number of APBs. In contrast, the number of APBs increased upon RNAi-mediated knockdown of high-mobility group nucleosome binding domain 5 (HMGN5), which counteracts the chromatin-condensing activity of linker histones (Rochman et al., 2009). Thus, the targeting of various chromatin modifiers had a significant effect on APB formation.

This prompted us to further investigate the role of the telomeric chromatin state in the ALT pathway. We evaluated differences in telomere compaction as reflected by the telomere repeat density. This parameter was derived from telomere FISH images by dividing the intensity of a Cy3-labeled focal telomere repeat by its volume. To evaluate whether changes in telomere repeat compaction affected TRF2 binding to telomeres, we determined the ratio of TRF2 density to telomere repeat density from colocalizing TRF2 immunofluorescence and telomere FISH signals. The measured TRF2 to telomere repeat ratio was then corrected for the slightly reduced accessibility of the TRF2 antibody to telomere repeats of higher density as described in supplementary material Fig. S4. In this manner, we were able to compare TRF2 binding to telomere repeats at specific telomeres within one cell for different treatments. Next, we induced chromatin decondensation by treatment with the histone deacetylase inhibitor SAHA (Bradner et al., 2010; Choudhary et al., 2009; Tóth et al., 2004). Treatment with SAHA significantly reduced the telomere repeat density (P<0.001, Fig. 2A). The observed reduction in telomere repeat density after SAHA treatment was accompanied by a small, but statistically significant, increase in TRF2 binding per telomere repeat (P<0.01, Fig. 2B). Furthermore, SAHA strongly decreased the number of APBs per cell (mean±s.e.m., –49.4±6.9%, P<0.001, Fig. 2C) and C-circle levels (–45.3±10.3%, P<0.001, Fig. 2D).

We next employed a previously introduced technique to induce the *de novo* formation of ectopic APBs by recruiting GFP-tagged proteins to three telomeres in U2OS cells with stably integrated *lac* operator (*lac*O) arrays (Chung et al., 2011; Jegou et al., 2009). As controls, GFP alone was recruited (Fig. 2E) and a cell line with pericentric *lac*O array integration sites was used. HMGN5, as a factor that decondenses chromatin, and HP1γ, as a protein that promotes heterochromatin formation, were recruited (Fig. 2F,G). The capability of the two proteins to promote APB formation was monitored by the enrichment of endogenous PML protein at the telomeric *lac*O arrays. Recruitment of HMGN5 resulted in strong

Table 2. Quantitative telomere FISH analysis on metaphase spreads after 30 days of PML knockdown

	Median telomere repeat intensity without ECTRs (a.u.)	Median telomere repeat intensity with ECTRs (a.u.)	Telomere-free ends (%)	ECTRs per metaphase spread	Telomere repeat intensity of ECTRs (a.u.)	ECTR fraction of total telomere repeat intensity (%)
Uninduced	122.7±9.1	119.1±9.8	12.0±1.1	19.1±2.4	78.2±9.1	6.6±2.3
Induced PML knockdown	99.9±9.1	99.5±9.4	18.3±2.7	7.7±1.7	93.6±16.3	2.7±0.8
Difference between induced and uninduced (%)	–18.6±9.6**,[a]	–16.5±10.5**,[a]	52.5±26.5*,[b]	–59.8±10.2**,[b]	19.6±14.4*,[a]	–59.6±18.3[b]

Results are mean±s.e.m (n=20 metaphase spreads per treatment). *P<0.05; **P<0.001. [a]Kolmogorov-Smirnov test was used for statistical analysis; [b]Welch's t-test was used for statistical analysis.

Journal of Cell Science

Journal of Cell Science (2015) 128, 1887-1900 doi:10.1242/jcs.148296

Table 3. Proteins identified in the RNAi screen that significantly affected the number of APBs per cell

siRNA phenotype	Telomere organization	Protein sumoylation	DNA repair	Chromatin organization	Other biological processes
Less APBs	TIN2	MMS21[b] SUMO1/2/3[b] UBC9	BLM[c] ERCC4[c] FEN1[c] PARP2 XRCC6[c]	DNMT1 HDAC7 HP1γ LSD1 SUV420H2	CDKN1A MORC3 NR2C2 NR2F2 PML TOP3A
More APBs	POT1 TRF1[a]	SENP6	FANCD2 FANCL PCNA[c] RPA1[c] RPA2[c]	HMGN5	

A protein was considered as a hit in the screen if knockdown by two different siRNAs consistently changed the number of APBs by>10% ($P< 0.05$). According to associated biological processes defined by gene ontology (GO), hits were grouped into proteins involved in telomere organization (GO:0032200), protein sumoylation (GO:0016925), DNA repair (GO:0006281) and chromatin organization (GO:0006325). Hits that are annotated with more than one of these GO terms are indicated. [a]TRF1 is also annotated with the GO term 'chromatin organization'; [b]MMS21 und SUMO are also annotated with the GO term 'DNA repair'; [c]these proteins are also annotated with the GO term 'telomere organization'.

chromatin decondensation at the telomeric *lac*O arrays, as assessed by the formation of extended structures with irregular shape, which has previously been reported for non-telomeric *lac*O arrays (Rochman et al., 2009). No APBs could be detected at the telomeres of these cells, whereas 24±5% of *lac*O sequences were associated with APBs in the control cells ($P<0.001$, Fig. 2F). In contrast, recruiting GFP–HP1γ to the telomeric *lac*O arrays induced the subsequent enrichment of endogenous PML protein at the telomeres in a highly efficient manner, yielding 76±11% colocalization ($P<0.001$, Fig. 2G). PML enrichment upon HP1γ recruitment could be due to SUMO-mediated interactions as discussed previously (Lang et al., 2010) or could occur through SP100 (Seeler et al., 1998), a known interaction partner of PML. Notably, PML enrichment was accompanied by the induction of repair-associated DNA synthesis, as concluded from the increased levels of the phosphorylated histone variant H2A.X (γH2A.X) and of incorporated 5-bromo-2'-deoxyuridine (BrdU) (Fig. 2H,I). This effect was specific for telomeric *lac*O arrays. Recruitment of HP1γ to pericentric *lac*O arrays had no significant effect on the level of γH2A.X (Fig. 2J). Taken together, decondensation of telomeric chromatin inhibited APB formation, whereas a compacted chromatin state was found to be compatible with both APB formation as well as repair-associated DNA synthesis at telomeres.

Telomere repeat density is increased in APBs whereas TRF2 binding to telomeres is decreased

To investigate differences in the level of compaction at single telomeres in unperturbed ALT cells, we analyzed the telomere repeat density in APBs as compared to telomere repeat foci that were not located in APBs. The median telomere repeat density in APBs was 2.6±0.1-fold higher as compared to telomeres outside APBs ($P<0.001$, Fig. 3A). To distinguish whether APBs induce compaction of telomeric chromatin or whether they assemble at pre-existing highly dense telomeres, the effect of short-term PML knockdown on the telomere repeat density was evaluated (Table 1). The median telomere repeat density was significantly reduced by 9.9±3.4% (mean±s.e.m.) after PML knockdown. This indicates that the increased compaction of telomere repeats was induced by APBs and was maintained only as long as PML was present.

Next, we evaluated whether the APB-mediated increase of the telomere repeat density influenced TRF2 binding to these telomeres. The ratio of the TRF2 density to telomere repeat density was strongly decreased in APBs as compared to telomeres that were not located in APBs (median, –35.2±4.9%, $P<0.001$, Fig. 3B). Thus, telomeres in APBs had less TRF2 bound per telomere repeat. Interestingly, telomere repeat density was inversely correlated with TRF2 binding: the least-dense telomeres had 2.6±0.7-fold more TRF2 bound per telomere repeat as compared to the densest telomere ($P<0.001$, Fig. 3C). This value includes the above-mentioned correction for differences in antibody accessibility (supplementary material Fig. S4G). To confirm that PML was required for the reduced binding of TRF2 at telomeres in APBs, we measured TRF2 binding to telomere repeats before and after PML knockdown. Notably, PML knockdown increased the amount of TRF2 bound per telomere repeat by ~40% (Table 1). No change in the mean integrated TRF2 immunofluorescence signal per cell was detected, indicating that TRF2 levels per cell remained unaffected. Thus, we conclude that APBs induce a compaction of telomeric chromatin that correlates with reduced binding of TRF2 per telomere repeat.

The SUMO E3 ligase MMS21 and PARP-2 modulate TRF2 binding to telomeres in APBs

Next, we investigated whether knockdown of proteins involved in post-translational modifications of shelterin proteins affected the binding of TRF2 to telomeres in APBs. The ratio of TRF2 signal to the telomere repeat signal (i.e. the coverage of telomere repeats with TRF2) was affected inside APBs upon knockdown of two different post-translational modifiers of TRF2, which have been reported to be enriched in APBs (Dantzer et al., 2004; Potts and Yu, 2007). First, knockdown of the SUMO E3 ligase MMS21, which sumoylates the shelterin components TRF1, TRF2, TIN2 and RAP1 (Potts and Yu, 2007), increased TRF2 binding to telomeres in APBs by 18.1±1.9% (mean±s.e.m., $P<0.001$). The opposite effect on the ratio of the TRF2 signal to the telomere repeat signal was observed for the knockdown of the SUMO protease SENP6, whereas other SENPs had no effect or decreased TRF2 binding to telomere repeats. Second, knockdown of poly(ADP-ribose) polymerase 2 (PARP-2) increased the ratio of the TRF2 signal to the telomere repeat signal in APBs by 9.3±0.3% ($P<0.001$) without affecting the telomere repeat density. Thus, post-translational modifiers of TRF2 that are known to be present in APBs can affect the amount of TRF2 that is bound per telomere repeat in APBs.

Journal of Cell Science (2015) 128, 1887-1900 doi:10.1242/jcs.148296

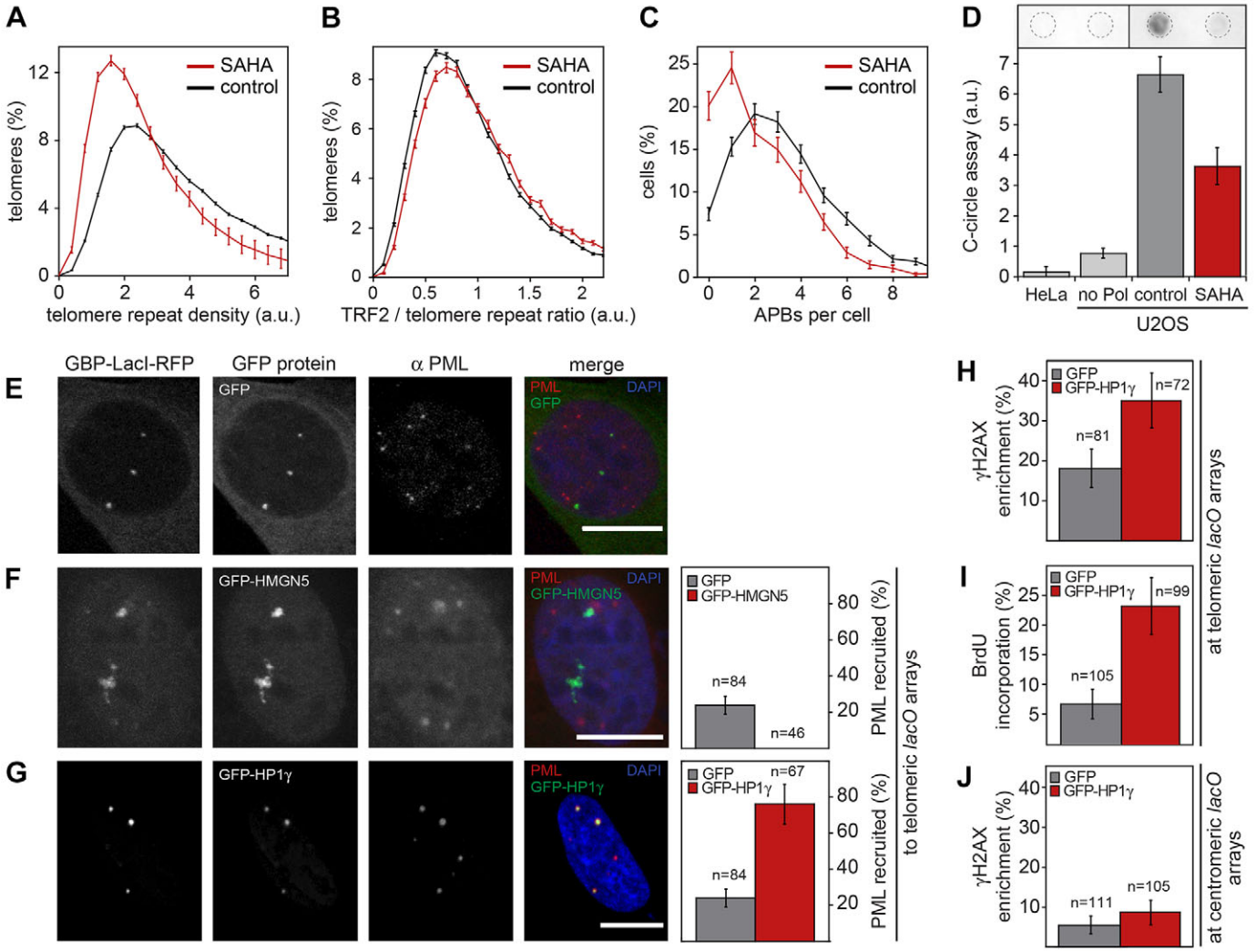

Fig. 2. Chromatin decondensation increases TRF2 binding to telomere repeats and reduces ALT features. (A) Relative frequency distributions of the telomere repeat densities, that is the fluorescence intensities of the Cy3-labeled telomeric FISH probe per volume, in U2OS cells (control, only ethanol solvent was added instead of SAHA) and in U2OS cells treated with 2 µM histone deacetylase inhibitor SAHA for 24 h. At least 47,300 telomeres were analyzed per experiment. (B) Relative frequency distributions of the ratio of TRF2 signal to the telomere repeat signal for control and SAHA-treated cells. The TRF2:telomere-repeat ratio was determined by dividing the density of the TRF2 immunofluorescence signal by the density of the colocalizing telomere FISH repeat signal. (C) Quantification of the number of APBs per cell. At least 700 cells were analyzed per treatment. (D) C-circle levels in control and SAHA-treated cells. As negative controls, a C-circle assay was performed with DNA of ALT-negative HeLa cells and with U2OS DNA lacking polymerase (no Pol) (*n*=9). Two segments from the same membrane were cut and assembled as indicated by the black line. (E–G) CLSM images of a U2OS cell line with *lac*O integrations at three telomeres. Cells were co-transfected with a GFP-binding protein (GBP) fused to the Lac repressor (LacI) (GBP–LacI–RFP, column 1) and the indicated GFP fusion protein (column 2), and immunostained for endogenous PML protein to quantify PML enrichment (column 3). (E) As a control, GFP was recruited to the *lacO* arrays allowing visualization of these as condensed spots. (F) Recruitment of GFP–HMGN5 to the telomeric *lacO* arrays. The graph shown on the right represents the mean percentage of colocalization between recruited GFP–HMGN5 and endogenous PML in comparison to control (GFP recruitment). (G) Recruitment of GFP–HP1γ to the telomeric *lacO* arrays. The graph shown on the right represents the mean percentage of colocalization between recruited GFP-HP1γ and endogenous PML in comparison to control. Scale bars: 10 µm. (H) Quantification of the enrichment of phosphorylated histone variant γH2A.X, a marker of double-strand break repair, at telomeric *lacO* arrays upon GFP–HP1γ recruitment. (I) Quantification of BrdU incorporation, as a marker for DNA synthesis, upon recruitment of GFP–HP1γ. Only cells with less than three BrdU foci were analyzed to exclude S-phase cells with replication-dependent BrdU incorporation. (J) Same as H, but at centromeric *lac*O arrays. Quantitative results represent mean±s.e.m.

APBs induce enrichment of phosphorylated ATM at high-density telomeres

TRF2 is the main repressor of DNA damage response (DDR) at telomeres because it inhibits the autophosphorylation of the ATM kinase and its concomitant dissociation into monomers, the presumed active form of the kinase (Bakkenist and Kastan, 2003; Takai et al., 2003). As TRF2 binding to telomeres was strongly reduced in APBs (Fig. 3B), we addressed the question of whether this leads to the activation of ATM by autophosphorylation. Consistent with a previous report (Stagno D'Alcontres et al., 2007), the phosphorylated form of ATM (p-ATM) colocalized with APBs in U2OS cells (Fig. 4A, row 1). A quantitative analysis revealed that p-ATM was significantly enriched at telomeres associated with PML (Fig. 4B). Although only ∼2% of all telomeres colocalized with p-ATM, this fraction was significantly increased among telomeres in APBs. Approximately 15% of all APBs colocalized with p-ATM, indicating that the DDR was only activated in a specific subset of APBs (Fig. 4B). The median telomere repeat

Journal of Cell Science

Journal of Cell Science (2015) 128, 1887-1900 doi:10.1242/jcs.148296

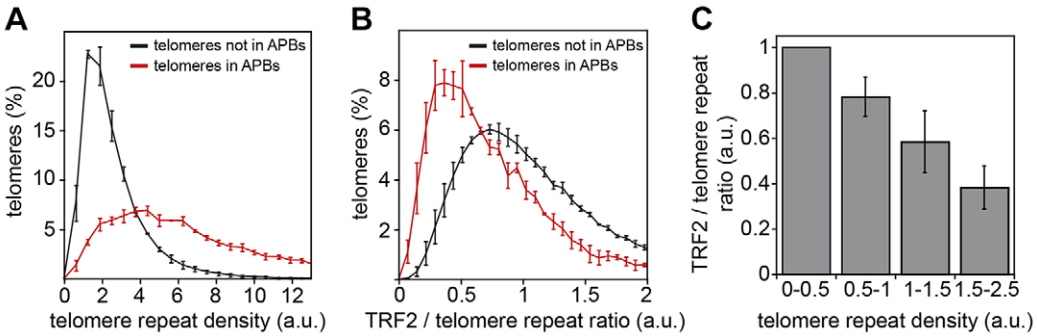

Fig. 3. Telomere repeat density is increased in APBs, while TRF2 binding to telomeres is decreased. (A) Relative frequency distributions of telomere repeat densities in U2OS cells in and outside of APBs. (B) Relative frequency distributions of the TRF2 to telomere repeat ratios (i.e. the amount of TRF2 per telomere repeat) of telomeres in relation to PML localization. The slightly reduced accessibility of the TRF2 antibody due to compaction of the telomere repeats was corrected for as described in supplementary material Fig. S4. For A and B, a total of 7487 telomeres in APBs and 130,025 telomeres that were not in APBs were analyzed. (C) Normalized median for the ratio of the TRF2 signal to telomere repeat signal for each of the indicated telomere repeat density ranges (n=137,512 telomeres). Results represent mean±s.e.m.

density in APBs with p-ATM was ~2.4 times higher than the density in APBs without p-ATM and even ~5.7 times higher than at telomeres that were not located in APBs (Fig. 4C). As shown in Fig. 3C, telomeres with the highest telomere repeat density had the lowest levels of bound TRF2. Thus, we conclude that ATM was only activated at telomeres in APBs with the highest telomere repeat densities and the lowest TRF2 levels.

To distinguish whether APBs enrich phosphorylated ATM at telomeres or whether APBs form at telomeres where the DDR is already activated, we analyzed the p-ATM distribution after 1 week of PML knockdown. The knockdown of PML increased the total number of p-ATM foci (+102±7%, mean±s.e.m., P<0.001, Fig. 4A,D), which is likely to reflect the previously reported general role of PML in DNA repair (Bernardi and Pandolfi, 2007). However, whereas in control cells about a quarter of all p-ATM foci were found at telomeres, the number of p-ATM foci at telomeres was strongly reduced after PML knockdown (–90±8%, mean±s.e.m., P<0.001, Fig. 4D). This indicates that ATM becomes activated at telomeres after APB formation rather than inducing the formation of APBs at telomeres where the DDR was already initiated. In support of this conclusion, ATM knockdown had no significant effect on the number of APBs (supplementary material Table S2). As reported previously, ATM interacts with the MRN 'damage sensor' complex, which leads to the recruitment of other repair proteins like MDC1 and 53BP1 (Derheimer and Kastan, 2010). Although these proteins are known to colocalize with APBs (Jiang et al., 2007), their knockdown had no effect on the number of APBs in our screen (supplementary material Table S2), implying that a functional DDR was not necessary for APB formation.

Next, we evaluated whether APB-induced ATM phosphorylation was necessary for telomere elongation by inhibiting ATM for 4 weeks with KU-55933 (Hickson et al., 2004). This treatment reduced the number and density of p-ATM foci by 45.2±2.1% and 48.2±3.6%, respectively (P<0.001). Furthermore, the amount of C-circles was reduced after treatment with the ATM inhibitor (–33.6±10.8%, P<0.05, Fig. 4E). Notably, the median fluorescence intensity of the Cy3-labeled telomere repeats (–12.9±2.7%, P<0.001, Fig. 4F) decreased without significantly affecting the number of APBs per cell (+2.8±3.5%, P>0.1). Thus, ATM inhibition correlated with a loss of telomere repeats, but did not affect APB formation. This indicates that ATM activation in APBs promotes subsequent DNA-repair-associated telomere elongation.

DISCUSSION

In the present study, we investigated the link between APB formation, TRF2 binding to telomeres and telomere lengthening in the ALT-positive U2OS cell line. Based on our findings, we propose a model for APB-mediated telomere lengthening that involves the following main steps and integrates findings from previous studies (Fig. 5). First, formation of a PML subcompartment at telomeres induces telomeric chromatin compaction and clustering of telomeres, and possibly also ECTRs, as proposed previously (Cho et al., 2014; Draskovic et al., 2009). Second, as a result of APB formation, TRF2 becomes partly depleted at associated telomeres. This process could involve post-translational modifications of TRF2, such as sumoylation by MMS21 or poly-ADP ribosylation by PARP-2, in line with previous studies (Dantzer et al., 2004; Potts and Yu, 2007). Third, the reduced TRF2 density triggers autophosphorylation of ATM in APBs and DDR according to the previously identified role of TRF2 as an inhibitor of ATM (Denchi and de Lange, 2007; Karlseder et al., 2004). Fourth, telomeres are elongated by repair-associated DNA synthesis and recombination events that are promoted by telomere clustering in APBs. Finally, as APBs disassemble, repair and recombination factors dislocate, telomeres are released and telomere density decreases again. This process leads to a re-enrichment of TRF2 that protects the extended telomeres from chromosomal fusions by non-homologous end joining (NHEJ).

Several lines of evidence support this model. An important role of APBs was established from the quantitative evaluation of the effect of PML knockdown in the ALT-positive U2OS cell line. Short-term PML knockdown for 72 h led to an almost complete loss of APBs, whereas the number of detectable telomere repeat foci increased by one to two for every APB that disappeared. This suggests clustering of two or three telomere repeat foci in one APB. Our Q-FISH interphase analysis did not reveal whether the additional telomere repeat foci observed after PML knockdown were telomeres or ECTRs. However, Q-FISH with a C-rich PNA probe on metaphase spreads showed that ECTRs accounted only for a relatively small fraction of the total telomere repeat intensity per cell. Furthermore, the number of detectable ECTRs was strongly reduced after PML knockdown. Thus, we conclude that the additional telomere repeat foci that appear after 72 h of PML knockdown arise mostly from telomeres. However, it is possible that ECTRs also contribute to the telomere repeat clusters inside APBs. Consistent with the view that APBs promote telomere clustering, it has been reported that telomeres attach to the surface of

Journal of Cell Science (2015) 128, 1887-1900 doi:10.1242/jcs.148296

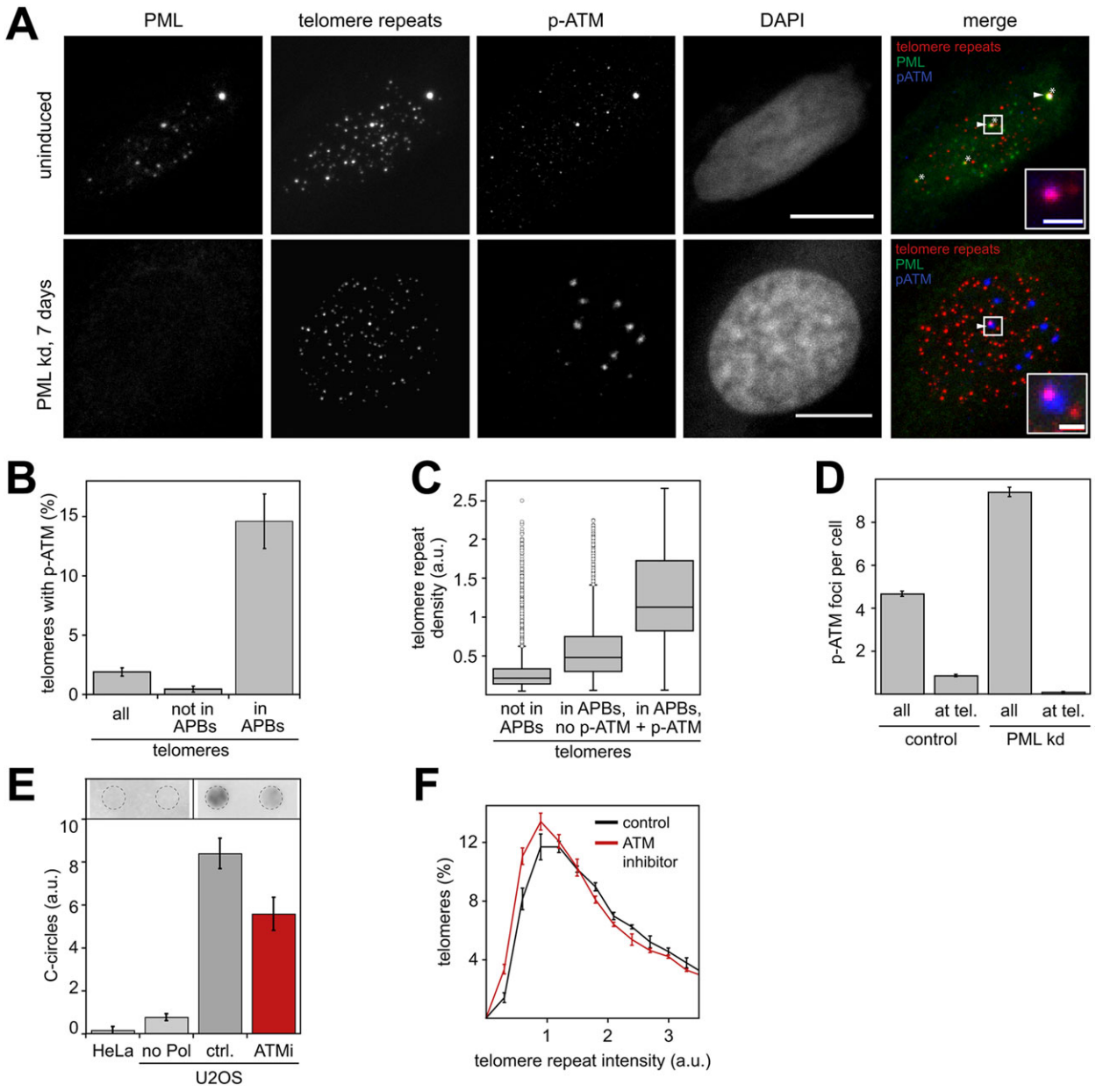

Fig. 4. ATM phosphorylation is induced at high-density telomere repeats inside APBs. (A) CLSM images of U2OS cells stained by immunofluorescence against PML and the activated ATM phosphorylated at S1981 (p-ATM), and with the Cy3-labeled telomeric FISH probe to visualize the telomeric repeats. Activated p-ATM colocalized with telomeres in APBs (top row). After 1 week of PML knockdown using the inducible U2OS cell line, fewer p-ATM foci colocalized with telomeres (bottom row). Arrowheads and stars indicate colocalization of p-ATM with telomeres and APBs, respectively. Scale bars: 10 µm (main images), 1 µm (inset). (B) Percentage of telomeres that colocalize with p-ATM. The number of p-ATM foci at all telomeres, at telomeres not in APBs and at telomeres in APBs was divided by the corresponding number of telomeres. The number of evaluated telomeres was 21,269 (all), 19,011 (not in APBs) and 2258 (in APBs). (C) Box plot of the telomere repeat densities in APBs with or without p-ATM in comparison to telomeres that lack PML. The box represents the 25–75th percentiles, and the median is indicated. The whiskers show the 10–90th percentiles. Outliers are indicated as circles. (D) Effect of PML knockdown on the number of p-ATM foci in total (all) and at telomeres. (E) C-circle levels after inhibition of ATM with 10 µM inhibitor KU-55933 for 48 h. ALT-negative HeLa cells and U2OS cells without addition of polymerase were used as negative controls. The graph represents the mean of six independent experiments. Two segments from the same membrane were cut and assembled as indicated by the black line. (F) Distribution of the telomere repeat intensities after 4 weeks of ATM inhibition as compared to control cells. At least 10,000 telomeres were analyzed per treatment. Quantitative results represent mean±s.e.m.

artificially enlarged APBs (Draskovic et al., 2009) and that damaged telomeres preferentially cluster with telomeres that are associated with PML in ALT-positive cells (Cho et al., 2014). Notably, long-term PML knockdown induced telomere shortening and significantly increased the number of chromosomal ends where a telomere repeat signal was absent. This demonstrates that PML is crucial for telomere elongation in ALT cells and confirms previous conclusions (Chung et al., 2011; Jiang et al., 2005). Although inhibition of the ALT mechanism by other means has been employed previously (Jiang et al., 2005; Potts and Yu, 2007), our study is the first to reveal the crucial contribution of PML by showing a telomere shortening upon its knockdown.

Having established the importance of PML for the ALT mechanism, we investigated the formation of APBs and their

Journal of Cell Science (2015) 128, 1887-1900 doi:10.1242/jcs.148296

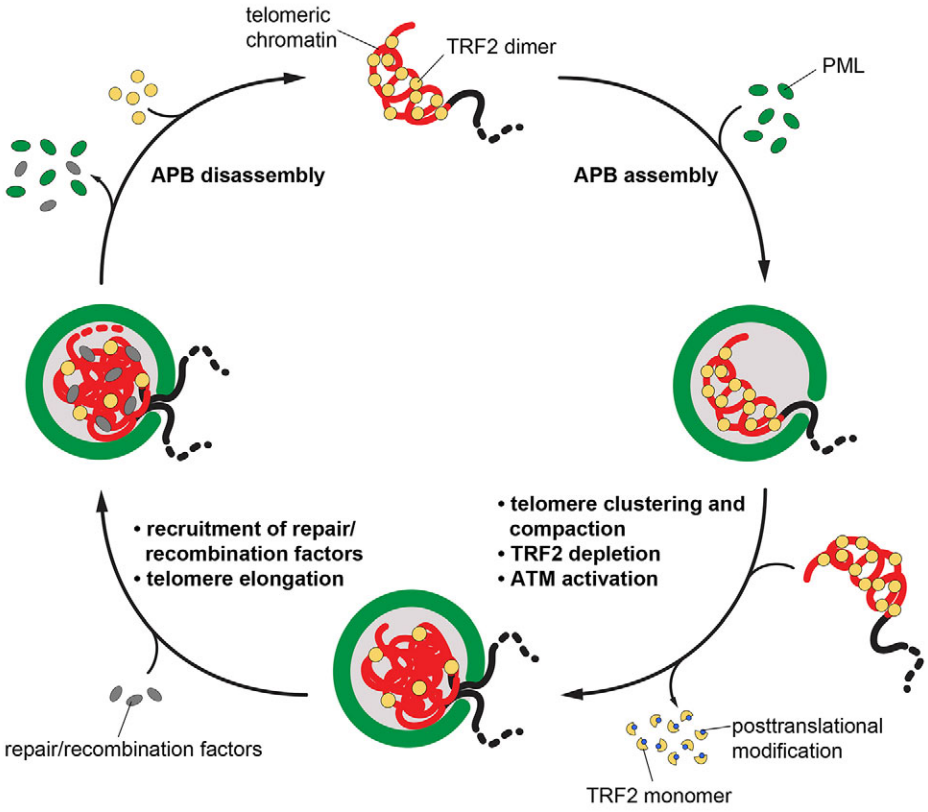

Fig. 5. Model for APB-mediated telomere elongation in ALT-positive cells. The formation of a PML subcompartment at telomeres induces telomeric chromatin compaction and clustering of telomeres, and possibly also ECTRs, as proposed previously (Cho et al., 2014; Draskovic et al., 2009). As a result of APB formation, TRF2 becomes partly depleted at associated telomeres. This process could involve the post-translational modifications of TRF2, such as sumoylation by MMS21 or poly-ADP ribosylation by PARP-2 in line with previous studies (Dantzer et al., 2004; Potts and Yu, 2007). These changes in telomere features trigger autophosphorylation of ATM in APBs and the DDR, in line with the previously identified role of TRF2 as an inhibitor of ATM (Denchi and de Lange, 2007; Karlseder et al., 2004). The subsequent recruitment of other DDR and DNA repair proteins to APBs promotes telomere elongation. Upon APB disassembly, repair and recombination factors dislocate, telomeres are released and telomere density decreases again. As a result, TRF2 binding is increased leading to the re-establishment of a fully protected telomere.

function in the ALT pathway with an automated quantitative 3D image acquisition and analysis approach in conjunction with RNAi-mediated knockdown. The quantification of individual telomeres and APBs from a total of more than 20 million images allowed us to identify 29 factors involved in APB formation and to elucidate the subsequent effects on telomere organization with unprecedented precision. The mechanism by which these factors operate is likely to involve direct effects that promote telomeric APB assembly as well as indirect effects related to DNA damage and its repair. Cell cycle effects appear to be less relevant in this context given that only very few tested siRNAs had significant effects on the cell cycle distribution. Note that proteins where the two targeting siRNAs showed inconsistent effects were not considered as hits in our screen (supplementary material Table S2). However, these proteins might nevertheless be involved in APB formation and the ALT mechanism as exemplified by the ataxia-telangiectasia- and RAD3-related (ATR) protein for which only one out of two siRNAs significantly reduced the number of APBs in our study. Indeed, a recent paper has shown that knockdown or inhibition of ATR specifically inhibits the ALT pathway and also reduces the number of APB-positive U2OS cells (Flynn et al., 2015). Knockdown of other DNA repair proteins, like the MRN complex components Rad50 and NBS1, as well as MDC1, 53BP1, BRCA1 and RAD51, did not affect the number of APBs for both siRNAs used, indicating that functional DDR and DNA repair pathways are not essential for APB formation (supplementary material Table S2). For 53BP1 and RAD51 knockdown, this is consistent with previous reports (Jiang et al., 2007; Potts and Yu, 2007). With respect to knockdown of RAD50 and NBS1, there is a disagreement with a previous study that reported a reduction in APB-positive IIICF/c cells upon knockdown of MRN components (Jiang et al., 2007). One reason could be that the abovementioned work used methionine-restriction-induced cell cycle arrest to artificially enrich the number of APBs. This treatment per se could have an impact on either APB formation or ALT. Accordingly, the effect of protein knockdown might be different from what is observed under the conditions used here for U2OS cells. A role for DNA repair proteins downstream of APB formation is also supported by our previous findings (Chung et al., 2011). Some repair proteins were inefficient in inducing the *de novo* formation of APBs, but instead were recruited to pre-assembled APBs. Note that the above results do not exclude the possibility that DNA damage also promotes the assembly of PML at telomeres in ALT-negative cells as reported previously (Hsu et al., 2012; Slatter et al., 2012).

The role of the telomeric chromatin state with respect to APB formation and telomere elongation in ALT cells is controversial. In telomerase-positive mice, it has been reported that knockout of several chromatin modifiers involved in heterochromatin formation results in APB formation and increased recombination at telomeres (Benetti et al., 2007; García-Cao et al., 2004; Gonzalo et al., 2006). To what extent these finding apply to human cells is unclear, given the differences in telomere biology between humans and mice (Calado and Dumitriu, 2013). Furthermore, a number of findings demonstrate that induction of a condensed heterochromatic state can even promote DNA repair and/or homologous recombination (Ayrapetov et al., 2014; Geuting et al., 2013). A recent study of DDR signaling in U2OS cells is particularly informative on this issue (Burgess et al., 2014). It shows that chromatin compaction is an integral part of DDR signaling and follows a transient chromatin expansion step.

We found here that APB assembly in U2OS cells was inhibited by an ‘open’ telomeric chromatin state, as the knockdown of several repressive chromatin modifiers, as well as chromatin decondensation initiated by HDAC inhibition or HMGN5 recruitment, resulted in a

Journal of Cell Science (2015) 128, 1887-1900 doi:10.1242/jcs.148296

significant reduction in the number of APBs (Fig. 2C,F). Previous work in ALT-positive IIICF/c cells has shown that HP1α (also known as CBX5) and HP1γ are needed for APB formation under methionine restriction and the authors hypothesized that HP1-mediated chromatin compaction is required for APB formation (Jiang et al., 2009). It was concluded that compacted telomeric DNA inside APBs would counteract telomere–telomere recombination. Here, we show that recruitment of HP1γ to telomeres is compatible with PML-induced DNA repair synthesis (Fig. 2H,I). This is in line with studies demonstrating the importance of HP1 family proteins for DNA repair and recombination, as discussed in several reviews (Cann and Dellaire, 2011; Dinant and Luijsterburg, 2009; Soria et al., 2012). Recently, it has been reported that chromatin compaction is globally reduced at ALT telomeres in comparison to telomeres in telomerase-positive cells (Episkopou et al., 2014). Our work focused on analyzing the compaction of single telomeres within an ALT cell line and has revealed differences in telomere repeat densities in relation to their association with PML (Fig. 3). In particular, we found that telomere repeats in APBs were more compact and bound less TRF2 than telomere repeats outside of APBs (Fig. 3B). Interestingly, the high telomere repeat densities observed in APBs correlated with the activation of a DNA damage response through ATM phosphorylation.

Previous reports have already speculated that partial telomere deprotection might be important for the repair-based ALT mechanism (Cesare et al., 2009; Cesare and Reddel, 2008; Nabetani et al., 2004). In particular, a lack of TRF2 at ALT telomeres has been proposed to be the cause of this deprotection, because the ratio of total TRF2 levels to the amount of telomeric DNA is significantly lower in ALT-positive cell lines compared to telomerase-positive cell lines (Cesare et al., 2009). Here, we specifically compared the ratio of TRF2 density to telomere repeat density as derived from colocalizing TRF2 immunofluorescence and telomere FISH signals at single telomeres in the ALT-positive U2OS cell line. This approach has allowed us to reveal differences in TRF2 binding to telomeres with or without APBs. Based on this comparison and the fact that PML knockdown led to reduced telomere repeat density and increased binding of TRF2, we propose that APBs are able to induce compaction of telomeric chromatin and reduce TRF2 levels at these telomeres.

A mechanism that could lead to a reduced binding of TRF2 to the telomere repeats in APBs is post-translational modification of TRF2 by the SUMO E3 ligase MMS21 and PARP-2, which have both been found to be enriched in APBs (Dantzer et al., 2004; Potts and Yu, 2007). In line with a previous study (Potts and Yu, 2007), knockdown of these proteins reduced APB formation in our RNAi screen. The relevance of sumoylation of shelterin and PML-NB components for PML-NB and APB formation has been described in a number of previous studies (Brouwer et al., 2009; Chung et al., 2011; Hattersley et al., 2011; Lang et al., 2010; Potts and Yu, 2007; Yu et al., 2010). Here, we additionally found that MMS21 knockdown increased TRF2 binding to telomeres in APBs, whereas knockdown of the SUMO protease SENP6 resulted in a decrease. Thus, our results support the previous hypothesis that recruitment of MMS21 to APBs leads to shelterin destabilization at these telomeres, possibly by interfering with TRF2 dimerization (Potts and Yu, 2007). Interestingly, knockdown of PARP-2 also increased the ratio of the TRF2 signal to the telomere repeat signal. It is known that PARP-2 covalently modifies the dimerization domain of TRF2 and non-covalently binds poly(ADP-ribose) to the MYB domain of TRF2, which decreases the DNA-binding affinity of TRF2 (Dantzer et al., 2004). Thus, the enrichment of MMS21 and PARP-2 in APBs could reduce the level of TRF2 bound to telomeres in APBs by interfering with TRF2 dimerization and DNA binding.

Short-term TRF2 depletion has previously been shown to increase the rate of telomeric sister chromatid exchanges (T-SCEs) (Zeng et al., 2009). However, TRF2 is also important for t-loop formation and prevents homologous-recombination-induced t-loop deletions and chromosome fusions mediated by NHEJ (Wang et al., 2004). In addition, long-term depletion of TRF2 in ALT cells leads to chromosome fusions by NHEJ, induction of senescence and telomere shortening due to uncontrolled recombination (Stagno D'Alcontres et al., 2007). Thus, we hypothesize that ALT cells depend on partial telomere deprotection to drive telomere recombination. At the same time, they need to prevent an extensive loss of TRF2, which would lead to telomere attrition and chromosome fusions as discussed previously (Cesare and Reddel, 2010). Based on the results described here, we conclude that APBs induce the formation of this 'intermediate-state'.

A previous report has shown that ATM is constitutively activated in ALT cells and colocalizes with APBs (Stagno D'Alcontres et al., 2007). Here, we show that ATM is preferentially activated in APBs that contain the densest telomere repeats. These highly dense telomere repeats had reduced levels of TRF2 bound per repeat. In addition, previous studies have found that TRF2 inhibits ATM by directly interacting with the region containing S1981, a residue whose autophosphorylation is necessary for the activation of this kinase (Denchi and de Lange, 2007; Karlseder et al., 2004). Accordingly, we propose that the reduction of TRF2 binding due to APB formation triggers ATM activation specifically at telomeres in APBs. The events subsequent to the DNA damage response, downstream of ATM-like recruitment of other DNA repair proteins and DNA repair synthesis (as detected by BrdU incorporation at APBs), have been addressed in our work that exploits ectopic APB assembly (Chung et al., 2011). Other studies have reported that multiple dysfunctional telomeres in ALT-positive cells colocalize with APB-like foci (Cesare et al., 2009) and that the phosphorylated histone H2AX (γH2AX), a molecular marker of double-strand breaks (DSBs) is found at some APBs (Nabetani et al., 2004). Here, we extended these observations by showing that PML knockdown reduced the number of telomeres colocalizing with p-ATM, whereas the total number of detectable p-ATM foci was increased (Fig. 4D). Thus, ATM was activated at telomeres after APBs were formed as opposed to a mechanism by which APBs assemble at telomeres where a DDR was already initiated. In addition, we found that inhibition of ATM did not affect the number of APBs, but decreased C-circle levels and reduced telomere repeat content, presumably due to a suppressed DDR at telomeres in APBs. In support of these results, it has been previously reported that ATM activity in ALT cells is not required for APB formation, but for telomeric DNA synthesis (Nabetani et al., 2004). Inhibiting the latter process in ALT cells does not have an immediate effect on cell viability and proliferation (Jiang et al., 2005; Potts and Yu, 2007). Consistent with this, ATM inhibition in U2OS cells hardly affects their survival on the time scale of several days, as is apparent from the experiments shown in Fig. 4 and in agreement with the findings from another study (Flynn et al., 2015).

In summary, our results demonstrate that PML induces compaction and confined TRF2 depletion at telomeres in APBs, and promotes telomere lengthening by initiating DNA damage signaling. Thus, APBs exert a central function in the disease phenotype of ALT-positive tumors.

Journal of Cell Science (2015) 128, 1887-1900 doi:10.1242/jcs.148296

MATERIALS AND METHODS

Plasmids

For the inducible PML knockdown, a double-stranded DNA (dsDNA) oligonucleotide consisting of a microRNA (miRNA) against PML was cloned into the pcDNA6.2-GW/EmGFPmiR vector (Invitrogen). The complete miRNA and emerald green fluorescent protein (EmGFP) coding sequence were then cloned into the inducible pT-Rex-DEST30 vector (Invitrogen). Sequences of the dsDNA oligonucleotides for PML knockdown were: top oligonucleotide: 5′-TGCTGTCTTGGATACAGCT-GCATCTTGTTTTGGCCACTGACTGACAAGATGCATGTATCCAAG-A-3′; and bottom oligonucleotide, 5′-CCTGTCTTGGATACATGCA-TCTTGTCAGTCAGTGGCCAAAACAAGATGCAGCTGTATCCAAG-AC-3′. The fluorescence three-hybrid system for recruiting GFP-tagged proteins to *lac*O arrays through GBP–LacI and GBP–LacI–RFP was used as described previously (Chung et al., 2011). The pEGFP-N2-mHMGN5 vector was kindly provided by Michael Bustin (Center for Cancer Research, National Cancer Institute, Bethesda, USA) (Rochman et al., 2009). The pEGFP-HP1γ plasmid was obtained by amplifying the human HP1γ cDNA sequence by PCR with an upstream forward primer, containing a BspEI restriction site, and a downstream reverse primer, containing a *Bam*HI restriction site. The PCR product was then cloned in pEGFP-C1 (Clontech, Palo Alto, CA).

Cell culture work

Human U2OS osteosarcoma cells (ATCC) and the U2OS cell clones with integrated *lacO* arrays, F6B2 and F42B8 (Jegou et al., 2009), were cultured in Dulbecco's modified Eagle's medium (DMEM; GIBCO) containing 10% fetal bovine serum (FBS; PAA) and 2 mM L-glutamine (PAA). The cell line stably expressing PML miRNA and EmGFP was constructed by co-transfection of the inducible pT-Rex-DEST30 vector containing a PML miRNA and EmGFP (Invitrogen) together with the Tet-repressor-coding vector pcDNA6/TR (Invitrogen). The selection was conducted with G418 and Blasticidin, and stable cell clones were picked and cultured for 10 days. The surviving cell clones were split into two fractions, and one fraction was maintained in doxycycline-free medium. For these cells, complete repression of the miRNA was ensured by analyzing GFP expression levels. The other fraction was induced with medium containing 1 µg/ml doxycycline (Sigma) for 24 h. The cell clone with the best repression in the uninduced state and best expression upon induction was used. The efficiency of PML knockdown was assessed by immunofluorescence against PML after 72 h of induction. For long-term PML knockdown, cells were cultured in medium containing 1 µg/ml doxycycline. Control cells were maintained in doxycycline-free medium. For the screening, 80,000 cells were seeded per slide on Lab-Tek chambered cover glasses (Thermo Scientific) and fixed after 72 h. For recruitment assays, cells were transfected using Effectene (Qiagen) according to the manufacturer's instructions and fixed after 24 h. For inhibition of histone deacetylases, cells were treated with 2 µM SAHA (Millipore) for 24 h and fixed afterwards. ATM was inhibited using 10 µM of the inhibitor KU-55933 (Hickson et al., 2004) (Calbiochem).

Immunofluorescence and FISH

After fixation with 4% paraformaldehyde in PBS for 12 min and washing three times with PBS, cells were permeabilized for 5 min with 0.1% Triton X-100 in PBS. After three PBS washes, cells were blocked for 1 h with 10% goat serum in PBS and afterwards incubated with primary antibody in 10% goat serum in PBS for 1 h. Cells were then washed three times with PBS containing 0.002% (v/v) NP-40. Subsequent staining with the appropriate secondary antibodies conjugated to fluorescent dyes was conducted for 1 h in 10% goat serum in PBS. After washing the cells three times with PBS, cells were mounted with ProLong Gold (Invitrogen) containing 4′,6-diamidino-2′-phenylindole (DAPI). The following antibodies were used: mouse anti-TRF2 (1:100, 4A794, Calbiochem), mouse anti-ATM phosphorylated at S1981 (1:100, #MAB3806, Millipore), mouse anti-Cy3/Cy5 (1:500, #ab52060, Abcam), rabbit anti-phospho-H2A.X (Ser139) (1:100, #07-164, Millipore), rabbit anti-PML (1:100, #sc-5621, Santa Cruz Biotechnology), mouse anti-BrdU (1:50, B44, BD Biosciences), goat anti-mouse-IgG conjugated to Alexa Fluor 488 (1:300, Invitrogen), goat anti-mouse-IgG conjugated to Alexa Fluor 568 (1:300, Invitrogen), goat anti-rabbit-IgG conjugated to Alexa Fluor 488 (1:300, Invitrogen) and goat anti-rabbit-IgG conjugated to Alexa Fluor 633 (1:200, Invitrogen).

For 5-bromo-2'-deoxyuridine (BrdU) staining, cells were seeded, transfected and incubated for 2 days. After adding 100 µM BrdU (Sigma-Aldrich) to the medium for 2 h, cells were fixed and permeabilized with PBS containing 0.2% (v/v) Triton X-100. Cells were denatured with 1.5 M HCl for 30 min, blocked and stained with an antibody against BrdU as described above.

For telomere FISH, cells were washed three times with PBS and fixed with 4% paraformaldehyde in PBS for 12 min. After 5 min permeabilization with 0.2% (v/v) Triton X-100 in PBS, cells were dehydrated in a series of ethanol washes (70, 85 and 100% ethanol) for 2 min each. After air-drying, the samples were incubated with a Cy3-labeled $(CCCTAA)_3$ PNA probe (0.1 µM, Panagene Inc.) in 75% formamide in 20 mM NaCl, 20 mM Tris-HCl, 0.1% BSA, pH 7.4. Samples were denatured at 80°C for 3 min and hybridized overnight at 30°C. Slides were then washed consecutively with 70% formamide in 10 mM Tris-HCl pH 7.4, 2× SSC, 0.1× SSC at 55°C and 0.05% Tween-20 in 2× SSC (v/v). Subsequent immunofluorescence was conducted as described above. Quantitative FISH on metaphase spreads (Q-FISH) was performed as described previously (Poon and Lansdorp, 2001).

Fluorescence microscopy and image analysis

Confocal fluorescence images were acquired with a Leica TCS SP5 DMI6000 confocal laser scanning microscope (oil immersion objective lens, 63×, 1.4 NA). The automated screening was conducted as described previously (Osterwald et al., 2012). For manual image acquisition, images were acquired with the Leica TCS SP5 DMI6000 confocal laser scanning microscope using the LAS AF software and parameters as described above. The automated image analysis was performed using a 3D-model-based segmentation approach (Osterwald et al., 2012; Wörz et al., 2010).

The relative frequency distributions in Fig. 1D, Fig. 2A–C, Fig. 3A, B and Fig. 4F were obtained by binning the data and plotting the relative frequencies of telomeres or cells in each bin together with the corresponding s.e.m. as data points connected by lines. The analysis of metaphase telomere FISH was performed with the automated image analysis pipeline described above. Interphase cells and telomere repeat foci not associated with chromosomes (ECTRs) were excluded from the analysis. The manual analysis of microscopy images was performed with the ImageJ software (http://rsbweb.nih.gov/ij). For the analysis of the recruitment efficiency to *lac*O arrays, spots were counted as colocalizing if the signal at the *lac*O array was at least twofold above the background and comprised at least two pixels with a size of 200 nm.

C-circle assay

The C-circle assay was performed as described previously (Henson et al., 2009). Briefly, DNA was isolated from 1×10^6 cells using the QIAamp DNA Mini Kit (Qiagen). DNA was quantified using a Qubit Fluorometer (Life Technologies). Genomic DNA (20 ng) was digested with 12.5 U/µg HinfI and RsaI restriction enzymes (both Roche) and 5000 ng/µg RNase A (Thermo Fisher Scientific) for 2 h at 37°C. The digested DNA (10 µl) was combined with 10 µl 1× Φ29 Buffer, 7.5 U Φ29 DNA polymerase (both NEB), 0.2 mg/ml BSA, 0.1% (v/v) Tween 20, 1 mM each dATP, dGTP and dTTP and incubated for 8 h at 30°C and then at 65°C for 20 min. After adding 40 µl 2× SSC, the sample was dot-blotted onto a 2×-SSC-soaked Roti-Nylon plus membrane (pore size 0.45 µm, Carl Roth). The membrane was baked for 20 min at 120°C and hybridized and developed using the TeloTAGGG Telomere Length Assay Kit (Roche). Intensities of C-circle dot blots were analyzed and background-corrected using Image Lab 4.1 (Bio-Rad).

TRF analysis and telomere-repeat quantitative PCR

Genomic DNA was purified using the Gentra Puregene Cell Kit (Qiagen). For terminal restriction fragment (TRF) analysis, 5 µg of purified DNA was digested with HinfI and RsaI overnight. The digested DNA was resolved on

a 0.6% agarose gel (Biozym Gold Agarose) in 1× TAE buffer using the CHEF-DRII pulsed-field gel electrophoresis system (Bio-Rad) with the following settings: 4 V/cm, initial switch time 1 s, final switch time 6 s, and 13 h duration. Southern blotting and chemiluminescent detection was performed using the TeloTAGGG Telomere Length Assay Kit (Roche) according to the manufacturer's instructions. The blot was visualized with a ChemiDoc MP imaging system (Bio-Rad). Approximate mean TRF lengths were quantified using ImageJ and according to the following equation: $\Sigma(OD_i)/\Sigma(OD_i/L_i)$, where OD_i is the optical density at position i and L_i is the TRF length at position i.

Telomere-repeat quantitative PCR was conducted essentially as described previously (Cawthon, 2002; O'Callaghan et al., 2008). In short, 5 or 10 ng DNA, 1× LightCycler 480 SYBR Green I Master (Roche), 500 nM forward primer and 500 nM reverse primer were added per 10 µl reaction. The primer sequences were: telo fwd, 5′-CGGTTTGTTTGGGTTTGGGTTTGGGT-TTGGGTTTGGGTT-3′; and telo rev, 5′-GGCTTGCCTTACCCTTACCC-TTACCCTTACCCTTACCCT-3′; 36B4 fwd, 5′-AGCAAGTGGGAAG-GTGTAATCC-3′; and 36B4 rev, 5′-CCCATTCTATCATCAACGGGT-ACAA-3′. Cycling conditions (for both telomere and 36B4 products) were 10 min at 95°C, followed by 40 cycles of 95°C for 15 s and 60°C for 1 min. A standard curve was used to determine relative quantities of telomere repeats (T) to that of a single copy gene (S, *36B4* gene, also known as *RPLP0*). The T:S ratio was calculated and normalized to a reference T:S ratio.

RNA interference

Transfected cell microarrays were produced as previously described (Erfle et al., 2007). Repetitions of a 4×4 array were printed on each Lab-Tek resulting in 384 spots with 24 replicates for each siRNA. A gene was considered as a hit if knockdown with two different siRNAs consistently affected the number of APBs by more than 10% (P<0.05). The experiments were conducted in triplicates, and 500 to 1500 cells were analyzed per siRNA. Sequences of all siRNAs (silencer select siRNAs, Ambion) as well as reported knockdown efficiencies, if available, can be found in supplementary material Table S1. The knockdown efficiencies of selected siRNAs that were important for further conclusions, namely CBX3, HDAC7, MRE11, NBS1, NSBP1, PARP2, RAD50, RAP1A, SENP6, SUV420H2 and TRF2, were validated by real-time quantitative PCR (supplementary material Fig. S3A). Values were normalized against β-actin. Primer sequences are provided in supplementary material Table S3. GO terms for biological processes associated with hits were identified by using the gene ontology website (http://geneontology.org).

Cell cycle analysis

To analyze the effect of each siRNA on the cell cycle, the background-corrected integrated DAPI intensities that were obtained in the automated high-content confocal screening were normalized and histograms were plotted (supplementary material Fig. S3B). As described previously, the distributions obtained in this manner correlate well with fluorescence-activated cell sorting (FACS) profiles (Tóth et al., 2004; Osterwald et al., 2012). Gates (e.g. for minimum and maximum DAPI intensity thresholds) were defined to obtain and compare the relative percentage of cells in G1, S and G2/M phase for each siRNA transfection. The same binning and gating was used for all conditions. The percentage of cells in each cell cycle phase was obtained from at least three replicates for each siRNA transfection. These data were used to calculate changes in the percentage of cells in G1, S and G2/M phase induced by each siRNA relative to control siRNA and the corresponding s.e.m.

Statistical analysis

The statistical analysis was conducted using the R software (http://www.r-project.org) as described previously (Osterwald et al., 2012). Errors bars always represent the s.e.m. of at least three independent experiments, unless stated otherwise. A Kolmogorov–Smirnov test was used to assess the significance of siRNA-related effects (supplementary material Table S2) and for the evaluation of interphase and metaphase FISH results with respect to changes in telomere repeat intensities or densities as well as TRF2: telomere repeat ratios. Welch's t-test was applied for the analysis of changes in cell cycle distribution, C-circle levels, the number of telomere-free ends, ECTRs and the percentage of ECTR intensity of total telomere intensity. For the analysis of the recruitment efficiency to *lac*O arrays, the percentage of *lacO* arrays with colocalization was determined with the indicated value n being the number of *lacO* arrays evaluated. Error bars were calculated as $\sqrt{n}$, which yields the standard deviation for a Poisson distribution. In order to determine whether the percentages of colocalization after recruiting the proteins of interest were significantly different from the ones obtained in the controls, the two-sided Fisher's exact test was used to calculate P-values.

Acknowledgements

We thank Nina Beil, Fabian Erdel, Delia Braun, Jürgen Reymann, Jana Molitor, Jan-Philipp Mallm and Brian Luke for help and discussions, and Michael Bustin for plasmid vectors.

Competing interests

The authors declare no competing or financial interests.

Author contributions

S.O., K.I.D. and K. Rippe designed the experiments. S.O., K.I.D., I.C. and D.P. performed experiments. S.W. and K. Rohr together with S.O. established the automated confocal imaging analysis platform. H.E. provided materials for reverse siRNA transfection and contributed to the establishment of the automated confocal image acquisition platform. S.O., K.I.D., I.C., D.P. and K. Rippe analyzed experiments and interpreted results. S.O., K.I.D., I.C. and K. Rippe wrote the manuscript.

Funding

The work of K. Rippe, K. Rohr and H.E. was funded within project CancerTelSys [grant number 01ZX1302] in the E:med program of the German Federal Ministry of Education and Research (BMBF). The ViroQuant-CellNetworks RNAi Screening Facility was supported by the CellNetworks-Cluster of Excellence [grant number EXC81].

Supplementary material

Supplementary material available online at
http://jcs.biologists.org/lookup/suppl/doi:10.1242/jcs.148296/-/DC1

References

Ayrapetov, M. K., Gursoy-Yuzugullu, O., Xu, C., Xu, Y. and Price, B. D. (2014). DNA double-strand breaks promote methylation of histone H3 on lysine 9 and transient formation of repressive chromatin. *Proc. Natl. Acad. Sci. USA* **111**, 9169-9174.

Bakkenist, C. J. and Kastan, M. B. (2003). DNA damage activates ATM through intermolecular autophosphorylation and dimer dissociation. *Nature* **421**, 499-506.

Benetti, R., Gonzalo, S., Jaco, I., Schotta, G., Klatt, P., Jenuwein, T. and Blasco, M. A. (2007). Suv4-20h deficiency results in telomere elongation and derepression of telomere recombination. *J. Cell Biol.* **178**, 925-936.

Bernardi, R. and Pandolfi, P. P. (2007). Structure, dynamics and functions of promyelocytic leukaemia nuclear bodies. *Nat. Rev. Mol. Cell Biol.* **8**, 1006-1016.

Bradner, J. E., West, N., Grachan, M. L., Greenberg, E. F., Haggarty, S. J., Warnow, T. and Mazitschek, R. (2010). Chemical phylogenetics of histone deacetylases. *Nat. Chem. Biol.* **6**, 238-243.

Brouwer, A. K., Schimmel, J., Wiegant, J. C., Vertegaal, A. C., Tanke, H. J. and Dirks, R. W. (2009). Telomeric DNA mediates de novo PML body formation. *Mol. Biol. Cell* **20**, 4804-4815.

Bryan, T. M., Englezou, A., Gupta, J., Bacchetti, S. and Reddel, R. R. (1995). Telomere elongation in immortal human cells without detectable telomerase activity. *EMBO J.* **14**, 4240-4248.

Bryan, T. M., Englezou, A., Dalla-Pozza, L., Dunham, M. A. and Reddel, R. R. (1997). Evidence for an alternative mechanism for maintaining telomere length in human tumors and tumor-derived cell lines. *Nat. Med.* **3**, 1271-1274.

Burgess, R. C., Burman, B., Kruhlak, M. J. and Misteli, T. (2014). Activation of DNA damage response signaling by condensed chromatin. *Cell Reports* **9**, 1703-1717.

Calado, R. T. and Dumitriu, B. (2013). Telomere dynamics in mice and humans. *Semin. Hematol.* **50**, 165-174.

Cann, K. L. and Dellaire, G. (2011). Heterochromatin and the DNA damage response: the need to relax. *Biochem. Cell Biol.* **89**, 45-60.

Cawthon, R. M. (2002). Telomere measurement by quantitative PCR. *Nucleic Acids Res.* **30**, e47.

Cesare, A. J. and Reddel, R. R. (2008). Telomere uncapping and alternative lengthening of telomeres. *Mech. Ageing Dev.* **129**, 99-108.

Cesare, A. J. and Reddel, R. R. (2010). Alternative lengthening of telomeres: models, mechanisms and implications. *Nat. Rev. Genet.* **11**, 319-330.

Journal of Cell Science

Cesare, A. J., Kaul, Z., Cohen, S. B., Napier, C. E., Pickett, H. A., Neumann, A. A. and Reddel, R. R. (2009). Spontaneous occurrence of telomeric DNA damage response in the absence of chromosome fusions. *Nat. Struct. Mol. Biol.* **16**, 1244-1251.

Cho, N. W., Dilley, R. L., Lampson, M. A. and Greenberg, R. A. (2014). Interchromosomal homology searches drive directional ALT telomere movement and synapsis. *Cell* **159**, 108-121.

Choudhary, C., Kumar, C., Gnad, F., Nielsen, M. L., Rehman, M., Walther, T. C., Olsen, J. V. and Mann, M. (2009). Lysine acetylation targets protein complexes and co-regulates major cellular functions. *Science* **325**, 834-840.

Chung, I., Leonhardt, H. and Rippe, K. (2011). De novo assembly of a PML nuclear subcompartment occurs through multiple pathways and induces telomere elongation. *J. Cell Sci.* **124**, 3603-3618.

Chung, I., Osterwald, S., Deeg, K. I. and Rippe, K. (2012). PML body meets telomere: the beginning of an ALTernate ending? *Nucleus* **3**, 263-275.

d'Adda di Fagagna, F., Reaper, P. M., Clay-Farrace, L., Fiegler, H., Carr, P., Von Zglinicki, T., Saretzki, G., Carter, N. P. and Jackson, S. P. (2003). A DNA damage checkpoint response in telomere-initiated senescence. *Nature* **426**, 194-198.

Dantzer, F., Giraud-Panis, M. J., Jaco, I., Amé, J. C., Schultz, I., Blasco, M., Koering, C. E., Gilson, E., Ménissier-de Murcia, J., de Murcia, G. et al. (2004). Functional interaction between poly(ADP-Ribose) polymerase 2 (PARP-2) and TRF2: PARP activity negatively regulates TRF2. *Mol. Cell. Biol.* **24**, 1595-1607.

Dellaire, G., Ching, R. W., Dehghani, H., Ren, Y. and Bazett-Jones, D. P. (2006). The number of PML nuclear bodies increases in early S phase by a fission mechanism. *J. Cell Sci.* **119**, 1026-1033.

Denchi, E. L. and de Lange, T. (2007). Protection of telomeres through independent control of ATM and ATR by TRF2 and POT1. *Nature* **448**, 1068-1071.

Derheimer, F. A. and Kastan, M. B. (2010). Multiple roles of ATM in monitoring and maintaining DNA integrity. *FEBS Lett.* **584**, 3675-3681.

Dinant, C. and Luijsterburg, M. S. (2009). The emerging role of HP1 in the DNA damage response. *Mol. Cell. Biol.* **29**, 6335-6340.

Draskovic, I., Arnoult, N., Steiner, V., Bacchetti, S., Lomonte, P. and Londoño-Vallejo, A. (2009). Probing PML body function in ALT cells reveals spatiotemporal requirements for telomere recombination. *Proc. Natl. Acad. Sci. USA* **106**, 15726-15731.

Episkopou, H., Draskovic, I., Van Beneden, A., Tilman, G., Mattiussi, M., Gobin, M., Arnoult, N., Londoño-Vallejo, A. and Decottignies, A. (2014). Alternative lengthening of telomeres is characterized by reduced compaction of telomeric chromatin. *Nucleic Acids Res.* **42**, 4391-4405.

Erfle, H., Neumann, B., Liebel, U., Rogers, P., Held, M., Walter, T., Ellenberg, J. and Pepperkok, R. (2007). Reverse transfection on cell arrays for high content screening microscopy. *Nat. Protoc.* **2**, 392-399.

Flynn, R. L., Cox, K. E., Jeitany, M., Wakimoto, H., Bryll, A. R., Ganem, N. J., Bersani, F., Pineda, J. R., Suvà, M. L., Benes, C. H. et al. (2015). Alternative lengthening of telomeres renders cancer cells hypersensitive to ATR inhibitors. *Science* **347**, 273-277.

García-Cao, M., O'Sullivan, R., Peters, A. H., Jenuwein, T. and Blasco, M. A. (2004). Epigenetic regulation of telomere length in mammalian cells by the Suv39h1 and Suv39h2 histone methyltransferases. *Nat. Genet.* **36**, 94-99.

Geuting, V., Reul, C. and Löbrich, M. (2013). ATM release at resected double-strand breaks provides heterochromatin reconstitution to facilitate homologous recombination. *PLoS Genet.* **9**, e1003667.

Gonzalo, S., Jaco, I., Fraga, M. F., Chen, T., Li, E., Esteller, M. and Blasco, M. A. (2006). DNA methyltransferases control telomere length and telomere recombination in mammalian cells. *Nat. Cell Biol.* **8**, 416-424.

Grobelny, J. V., Godwin, A. K. and Broccoli, D. (2000). ALT-associated PML bodies are present in viable cells and are enriched in cells in the G(2)/M phase of the cell cycle. *J. Cell Sci.* **113**, 4577-4585.

Hande, M. P., Balajee, A. S., Tchirkov, A., Wynshaw-Boris, A. and Lansdorp, P. M. (2001). Extra-chromosomal telomeric DNA in cells from Atm(-/-) mice and patients with ataxia-telangiectasia. *Hum. Mol. Genet.* **10**, 519-528.

Harley, C. B., Futcher, A. B. and Greider, C. W. (1990). Telomeres shorten during ageing of human fibroblasts. *Nature* **345**, 458-460.

Hattersley, N., Shen, L., Jaffray, E. G. and Hay, R. T. (2011). The SUMO protease SENP6 is a direct regulator of PML nuclear bodies. *Mol. Biol. Cell* **22**, 78-90.

Heaphy, C. M., de Wilde, R. F., Jiao, Y., Klein, A. P., Edil, B. H., Shi, C., Bettegowda, C., Rodriguez, F. J., Eberhart, C. G., Hebbar, S. et al. (2011). Altered telomeres in tumors with ATRX and DAXX mutations. *Science* **333**, 425.

Henson, J. D., Cao, Y., Huschtscha, L. I., Chang, A. C., Au, A. Y., Pickett, H. A. and Reddel, R. R. (2009). DNA C-circles are specific and quantifiable markers of alternative-lengthening-of-telomeres activity. *Nat. Biotechnol.* **27**, 1181-1185.

Hickson, I., Zhao, Y., Richardson, C. J., Green, S. J., Martin, N. M., Orr, A. I., Reaper, P. M., Jackson, S. P., Curtin, N. J. and Smith, G. C. (2004). Identification and characterization of a novel and specific inhibitor of the ataxia-telangiectasia mutated kinase ATM. *Cancer Res.* **64**, 9152-9159.

Hsu, J. K., Lin, T. and Tsai, R. Y. (2012). Nucleostemin prevents telomere damage by promoting PML-IV recruitment to SUMOylated TRF1. *J. Cell Biol.* **197**, 613-624.

Ishov, A. M., Sotnikov, A. G., Negorev, D., Vladimirova, O. V., Neff, N., Kamitani, T., Yeh, E. T., Strauss, J. F., 3rd and Maul, G. G. (1999). PML is critical for ND10 formation and recruits the PML-interacting protein daxx to this nuclear structure when modified by SUMO-1. *J. Cell Biol.* **147**, 221-234.

Jegou, T., Chung, I., Heuvelman, G., Wachsmuth, M., Görisch, S. M., Greulich-Bode, K. M., Boukamp, P., Lichter, P. and Rippe, K. (2009). Dynamics of telomeres and promyelocytic leukemia nuclear bodies in a telomerase-negative human cell line. *Mol. Biol. Cell* **20**, 2070-2082.

Jiang, W. Q., Zhong, Z. H., Henson, J. D., Neumann, A. A., Chang, A. C. and Reddel, R. R. (2005). Suppression of alternative lengthening of telomeres by Sp100-mediated sequestration of the MRE11/RAD50/NBS1 complex. *Mol. Cell. Biol.* **25**, 2708-2721.

Jiang, W. Q., Zhong, Z. H., Henson, J. D. and Reddel, R. R. (2007). Identification of candidate alternative lengthening of telomeres genes by methionine restriction and RNA interference. *Oncogene* **26**, 4635-4647.

Jiang, W. Q., Zhong, Z. H., Nguyen, A., Henson, J. D., Toouli, C. D., Braithwaite, A. W. and Reddel, R. R. (2009). Induction of alternative lengthening of telomeres-associated PML bodies by p53/p21 requires HP1 proteins. *J. Cell Biol.* **185**, 797-810.

Jiang, W. Q., Nguyen, A., Cao, Y., Chang, A. C. and Reddel, R. R. (2011). HP1-mediated formation of alternative lengthening of telomeres-associated PML bodies requires HIRA but not ASF1a. *PLoS ONE* **6**, e17036.

Kamranvar, S. A. and Masucci, M. G. (2011). The Epstein-Barr virus nuclear antigen-1 promotes telomere dysfunction via induction of oxidative stress. *Leukemia* **25**, 1017-1025.

Kamranvar, S. A., Chen, X. and Masucci, M. G. (2013). Telomere dysfunction and activation of alternative lengthening of telomeres in B-lymphocytes infected by Epstein-Barr virus. *Oncogene* **32**, 5522-5530.

Karlseder, J., Hoke, K., Mirzoeva, O. K., Bakkenist, C., Kastan, M. B., Petrini, J. H. and de Lange, T. (2004). The telomeric protein TRF2 binds the ATM kinase and can inhibit the ATM-dependent DNA damage response. *PLoS Biol.* **2**, e240.

Lang, M., Jegou, T., Chung, I., Richter, K., Münch, S., Udvarhelyi, A., Cremer, C., Hemmerich, P., Engelhardt, J., Hell, S. W. et al. (2010). Three-dimensional organization of promyelocytic leukemia nuclear bodies. *J. Cell Sci.* **123**, 392-400.

Londoño-Vallejo, J. A., Der-Sarkissian, H., Cazes, L., Bacchetti, S. and Reddel, R. R. (2004). Alternative lengthening of telomeres is characterized by high rates of telomeric exchange. *Cancer Res.* **64**, 2324-2327.

Lovejoy, C. A., Li, W., Reisenweber, S., Thongthip, S., Bruno, J., de Lange, T., De, S., Petrini, J. H., Sung, P. A., Jasin, M. et al.; **ALT Starr Cancer Consortium** (2012). Loss of ATRX, genome instability, and an altered DNA damage response are hallmarks of the alternative lengthening of telomeres pathway. *PLoS Genet.* **8**, e1002772.

Nabetani, A. and Ishikawa, F. (2011). Alternative lengthening of telomeres pathway: recombination-mediated telomere maintenance mechanism in human cells. *J. Biochem.* **149**, 5-14.

Nabetani, A., Yokoyama, O. and Ishikawa, F. (2004). Localization of hRad9, hHus1, hRad1, and hRad17 and caffeine-sensitive DNA replication at the alternative lengthening of telomeres-associated promyelocytic leukemia body. *J. Biol. Chem.* **279**, 25849-25857.

O'Callaghan, N., Dhillon, V., Thomas, P. and Fenech, M. (2008). A quantitative real-time PCR method for absolute telomere length. *Biotechniques* **44**, 807-809.

Osterwald, S., Wörz, S., Reymann, J., Sieckmann, F., Rohr, K., Erfle, H. and Rippe, K. (2012). A three-dimensional colocalization RNA interference screening platform to elucidate the alternative lengthening of telomeres pathway. *Biotechnol. J.* **7**, 103-116.

Poon, S. S. and Lansdorp, P. M. (2001). Quantitative fluorescence in situ hybridization (Q-FISH). *Curr. Protoc. Cell Biol.* **12**, 18.4.1-18.4.21.

Potts, P. R. and Yu, H. (2007). The SMC5/6 complex maintains telomere length in ALT cancer cells through SUMOylation of telomere-binding proteins. *Nat. Struct. Mol. Biol.* **14**, 581-590.

Rochman, M., Postnikov, Y., Correll, S., Malicet, C., Wincovitch, S., Karpova, T. S., McNally, J. G., Wu, X., Bubunenko, N. A., Grigoryev, S. et al. (2009). The interaction of NSBP1/HMGN5 with nucleosomes in euchromatin counteracts linker histone-mediated chromatin compaction and modulates transcription. *Mol. Cell* **35**, 642-656.

Schotta, G., Lachner, M., Sarma, K., Ebert, A., Sengupta, R., Reuter, G., Reinberg, D. and Jenuwein, T. (2004). A silencing pathway to induce H3-K9 and H4-K20 trimethylation at constitutive heterochromatin. *Genes Dev.* **18**, 1251-1262.

Seeler, J. S., Marchio, A., Sitterlin, D., Transy, C. and Dejean, A. (1998). Interaction of SP100 with HP1 proteins: a link between the promyelocytic leukemia-associated nuclear bodies and the chromatin compartment. *Proc. Natl. Acad. Sci. USA* **95**, 7316-7321.

Shay, J. W. and Bacchetti, S. (1997). A survey of telomerase activity in human cancer. *Eur. J. Cancer* **33**, 787-791.

Shi, Y., Lan, F., Matson, C., Mulligan, P., Whetstine, J. R., Cole, P. A., Casero, R. A. and Shi, Y. (2004). Histone demethylation mediated by the nuclear amine oxidase homolog LSD1. *Cell* **119**, 941-953.

Slatter, T. L., Tan, X., Yuen, Y. C., Gunningham, S., Ma, S. S., Daly, E., Packer, S., Devenish, C., Royds, J. A. and Hung, N. A. (2012). The alternative lengthening

of telomeres pathway may operate in non-neoplastic human cells. *J. Pathol.* **226**, 509-518.

Soria, G., Polo, S. E. and Almouzni, G. (2012). Prime, repair, restore: the active role of chromatin in the DNA damage response. *Mol. Cell* **46**, 722-734.

Stagno D'Alcontres, M., Mendez-Bermudez, A., Foxon, J. L., Royle, N. J. and Salomoni, P. (2007). Lack of TRF2 in ALT cells causes PML-dependent p53 activation and loss of telomeric DNA. *J. Cell Biol.* **179**, 855-867.

Takai, H., Smogorzewska, A. and de Lange, T. (2003). DNA damage foci at dysfunctional telomeres. *Curr. Biol.* **13**, 1549-1556.

Tavalai, N., Papior, P., Rechter, S., Leis, M. and Stamminger, T. (2006). Evidence for a role of the cellular ND10 protein PML in mediating intrinsic immunity against human cytomegalovirus infections. *J. Virol.* **80**, 8006-8018.

Tokutake, Y., Matsumoto, T., Watanabe, T., Maeda, S., Tahara, H., Sakamoto, S., Niida, H., Sugimoto, M., Ide, T. and Furuichi, Y. (1998). Extra-chromosomal telomere repeat DNA in telomerase-negative immortalized cell lines. *Biochem. Biophys. Res. Commun.* **247**, 765-772.

Tóth, K. F., Knoch, T. A., Wachsmuth, M., Frank-Stöhr, M., Stöhr, M., Bacher, C. P., Müller, G. and Rippe, K. (2004). Trichostatin A-induced histone acetylation causes decondensation of interphase chromatin. *J. Cell Sci.* **117**, 4277-4287.

Verschure, P. J., van der Kraan, I., de Leeuw, W., van der Vlag, J., Carpenter, A. E., Belmont, A. S. and van Driel, R. (2005). In vivo HP1 targeting causes large-scale chromatin condensation and enhanced histone lysine methylation. *Mol. Cell. Biol.* **25**, 4552-4564.

Wang, R. C., Smogorzewska, A. and de Lange, T. (2004). Homologous recombination generates T-loop-sized deletions at human telomeres. *Cell* **119**, 355-368.

Wörz, S., Sander, P., Pfannmöller, M., Rieker, R. J., Joos, S., Mechtersheimer, G., Boukamp, P., Lichter, P. and Rohr, K. (2010). 3D geometry-based quantification of colocalizations in multichannel 3D microscopy images of human soft tissue tumors. *IEEE Trans. Med. Imaging* **29**, 1474-1484.

Yeager, T. R., Neumann, A. A., Englezou, A., Huschtscha, L. I., Noble, J. R. and Reddel, R. R. (1999). Telomerase-negative immortalized human cells contain a novel type of promyelocytic leukemia (PML) body. *Cancer Res.* **59**, 4175-4179.

Yu, J., Lan, J., Wang, C., Wu, Q., Zhu, Y., Lai, X., Sun, J., Jin, C. and Huang, H. (2010). PML3 interacts with TRF1 and is essential for ALT-associated PML bodies assembly in U2OS cells. *Cancer Lett.* **291**, 177-186.

Zeng, S., Xiang, T., Pandita, T. K., Gonzalez-Suarez, I., Gonzalo, S., Harris, C. C. and Yang, Q. (2009). Telomere recombination requires the MUS81 endonuclease. *Nat. Cell Biol.* **11**, 616-623.

Zhong, S., Müller, S., Ronchetti, S., Freemont, P. S., Dejean, A. and Pandolfi, P. P. (2000). Role of SUMO-1-modified PML in nuclear body formation. *Blood* **95**, 2748-2752.

Supplementary material

PML induces compaction, TRF2 depletion and DNA damage signaling at telomeres and promotes their alternative lengthening

Sarah Osterwald, Katharina I. Deeg, Inn Chung, Daniel Parisotto, Stefan Wörz, Karl Rohr, Holger Erfle and Karsten Rippe

Supplementary figures

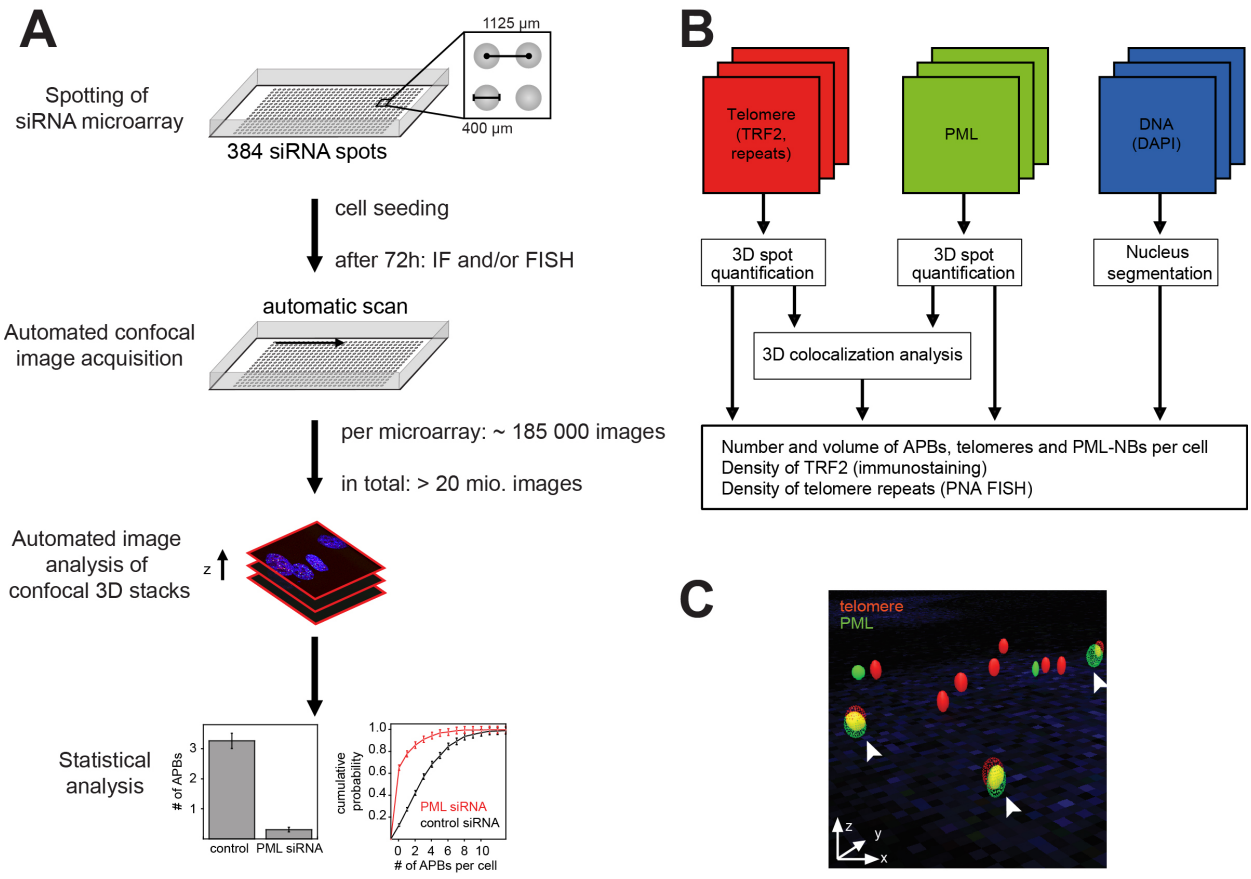

Fig. S1. Automated high-content 3D imaging and analysis platform for quantification of different ALT-related parameters.

(A) Workflow of the 3D colocalization RNAi screening platform. (B) Automated image analysis workflow and quantified parameters. (C) 3D visualization of telomere and PML colocalizations indicated by arrows.

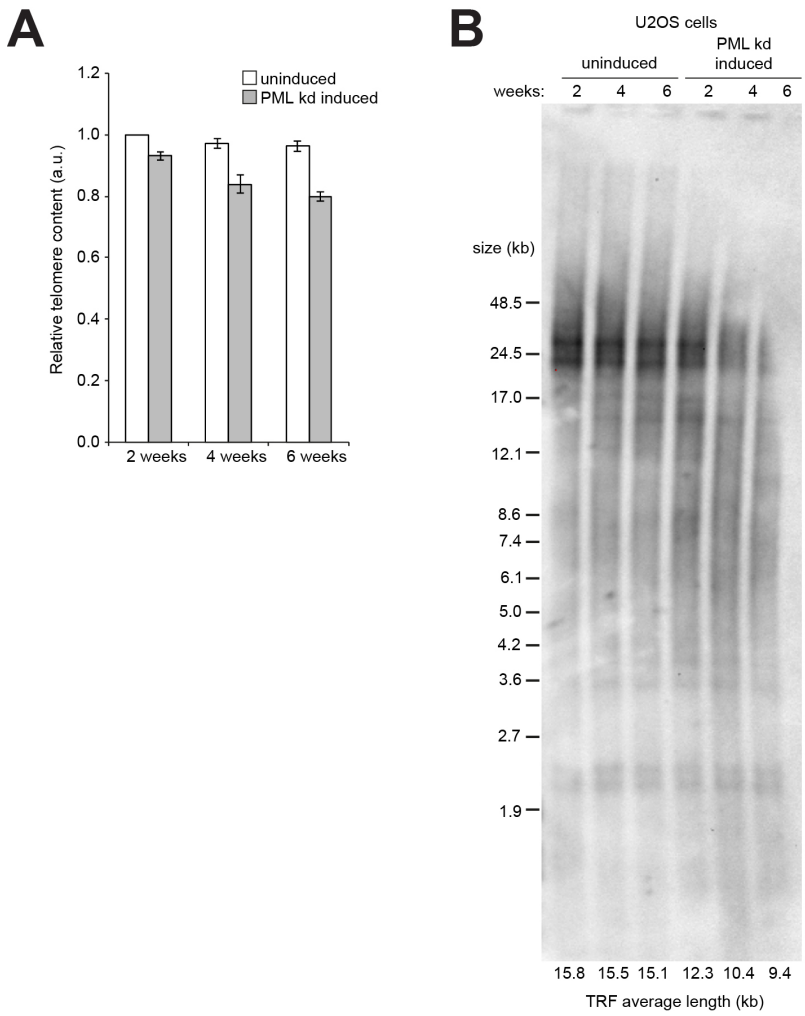

Fig. S2. Changes of telomere content and mean telomere length in U2OS cells upon long-term PML knockdown.

(A) Telomere repeat (*T*) and single copy *36B4* gene (*S*) quantitative PCR was performed with DNA from uninduced and PML knockdown induced U2OS cells cultured for 2, 4 or 6 weeks. A standard curve was used to determine relative quantities of *T* and *S*. The *T*/*S* ratio was calculated and normalized to the *T*/*S* ratio of uninduced U2OS cells cultured for 2 weeks. The relative telomere content is given as average of the normalized *T*/*S* ratios along with the s.e.m. of two independent experiments. (B) Terminal restriction fragment (TRF) analysis of uninduced or PML knockdown induced U2OS cells cultured for 2, 4 or 6 weeks. Mean TRF lengths were quantified using ImageJ and according to the equation: $\Sigma\ (OD_i) / \Sigma\ (OD_i/L_i)$, where OD_i is the optical density at position *i* and L_i is the TRF length at position *i*.

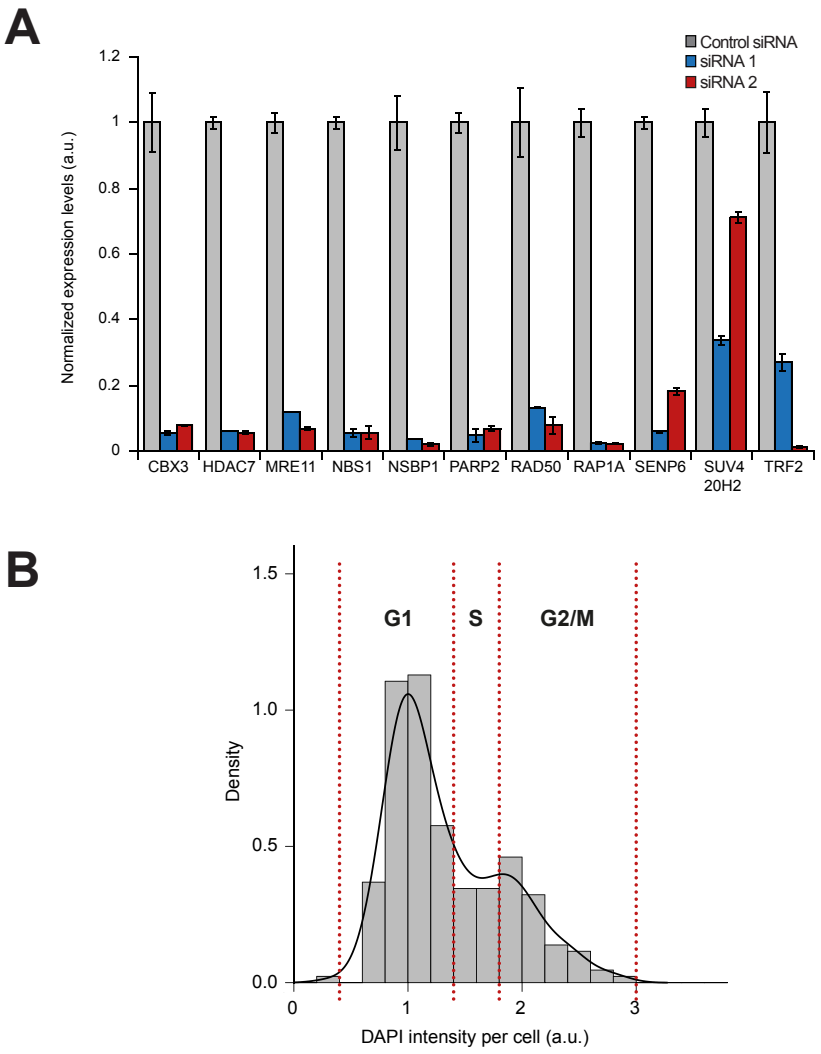

Fig. S3. Evaluation of siRNAs knockdown efficiency and cell cycle effects.

(A) U2OS cells were transfected with control or siRNAs and expression levels were measured by quantitative real-time PCR. Expression levels for each target were normalized against β-actin and are given as average percent mRNA remaining relative to negative control siRNA-treated samples along with the s.e.m. of three independent experiments. (B) For all siRNA hits the effect on the cell cycle was analyzed by generating cell cycle profiles from DAPI intensities**.** The integrated background corrected DAPI intensities of siRNA-transfected U2OS cells that were obtained from the high-content 3D confocal screen were normalized and binned. Gates were defined to obtain and compare the relative percentage of cells in G1, S and G2/M phase for every siRNA transfection. The same binning and gating was used for all samples. A representative histogram (light grey columns) and density profile (black line) of DAPI intensities of U2OS cells transfected with control siRNA is shown. The gates set for obtaining the percentage of cells in each cell cycle are represented by dashed red lines. The average cell cycle distribution of U2OS cells transfected with control siRNA as well as significant cell cycle changes of target siRNAs relative to control siRNA are provided in Supplementary Table 2.

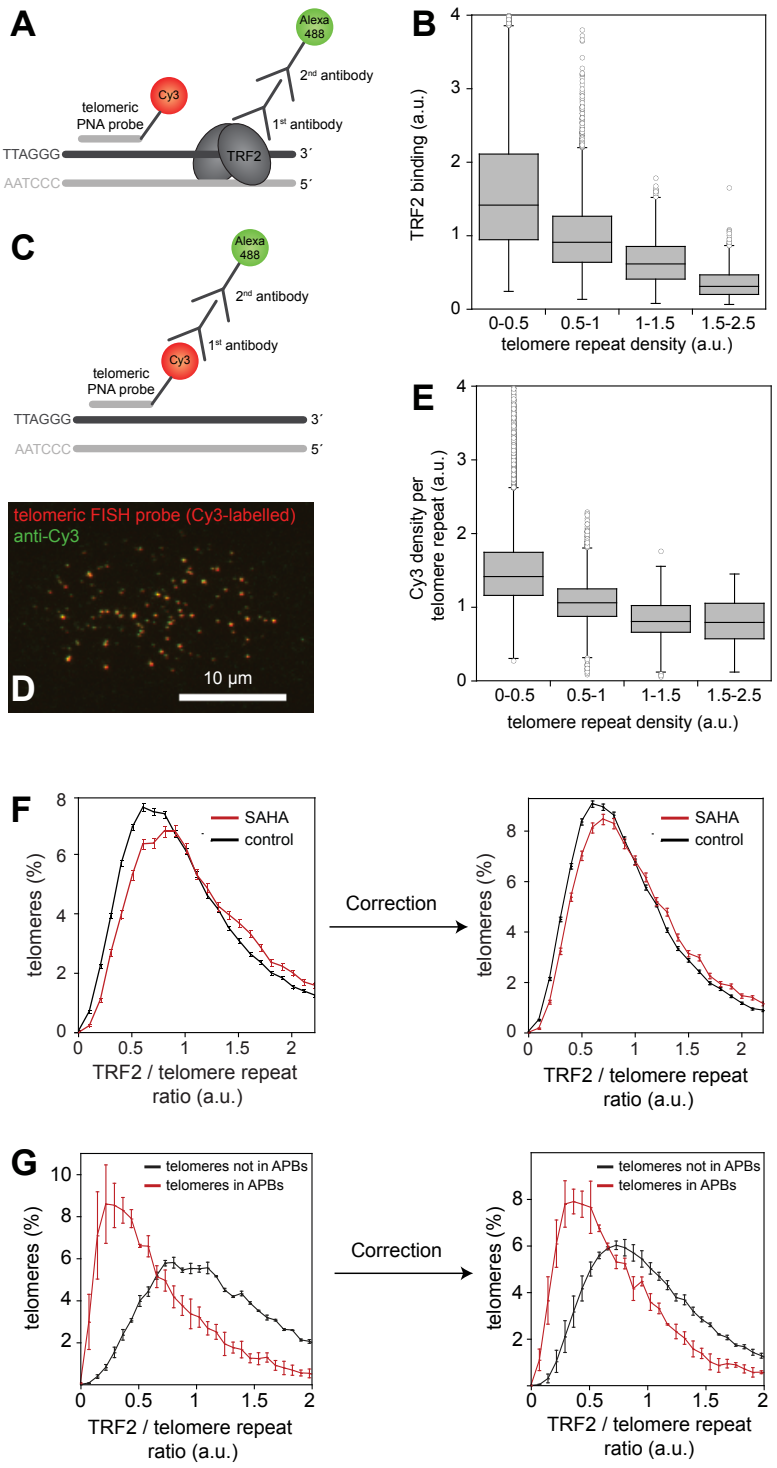

Fig. S4. Correction of differences in the accessibility of the TRF2 antibody and the Cy3-labeled telomeric FISH probe.

(A) The density of telomere repeats can be assessed with the Cy3-labeled telomeric FISH probe. For the detection of TRF2 by immunofluorescence, an unlabeled primary antibody against TRF2 was used together with an Alexa 488-labeled secondary antibody. (B) Box plot of bound TRF2 per telomere repeat in dependence of the corresponding telomere repeat density. TRF2 binding per telomere repeat was calculated by dividing the density of the TRF2 immunofluorescence signal through the colocalizing telomere FISH signal density. TRF2

binding to telomeres showed strong negative correlation with the telomere repeat density, i.e. telomeres with a high telomere repeat density bound less TRF2 (Spearman correlation coefficient = -0.5, $p < 0.001$). The densest telomeres bound 78.2 ± 0.2% less TRF2 as compared to the least dense telomeres. (C) To account for different accessibilities of the Cy3-labeled telomeric FISH probe as compared to the antibody-mediated immunofluorescent detection of TRF2, immunofluorescence against Cy3 was combined with FISH using the Cy3-labeled telomeric probe. If the FISH probe and the antibodies have the same accessibility, the Cy3 density per telomere repeat should be constant for different telomere repeat densities. (D) Confocal image of the co-localizing signals from the Cy3-labeled telomeric probe and the anti-Cy3 antibody. (E) The density of the anti-Cy3 antibody per telomere repeat was calculated and plotted against the respective telomere repeat density as determined by the Cy3-labeled telomeric probe. The density per telomere repeat of the anti-Cy3 antibody showed a weak negative correlation with the telomere repeat density. This reduction in antibody accessibility at dense telomeres was accounted for as follows: The measured densities of the anti-Cy3 antibody per telomere repeat were used to fit a correction curve in dependence of telomere repeat densities, resulting in individual correction factors for each telomere repeat density. These factors were used to correct the TRF2 binding per telomere repeat data that are depicted in Fig. 2B, 3B and 3C in the main text. (F) Relative frequency distributions of TRF2 / telomere repeat ratios as shown in Fig. 2B in the main text before and after correction. The TRF2 / telomere repeat ratio data was binned and the relative frequencies of telomeres in each bin together with the corresponding s.e.m. were plotted as data points connected by lines. (G) Same as panel F but for the data presented in Fig. 3B.

Supplementary table legends

Table S1. Sequences and knockdown efficiencies of the siRNAs used in the RNAi screen.

Two siRNAs for each target gene were used. The identification key listed with the sequence (Silencer select siRNA ID) refers to the silencer select siRNAs from Ambion that were used in the study. Where available, information on knockdown efficiencies of siRNAs is given. The table is provided as a separate Excel file.

Download Table S1

Table S2. Results of the RNAi screen.

Absolute average values and s.e.m. are given for U2OS cells transfected with control siRNA with respect to (i) number of APBs per cell, (ii) number of PML-NBs per cell, (iii) ratio of APBs to PML-NBs per cell, (iv) PML-NB volume, (v) number of TRF2 foci per cell, (vi) TRF2 volume, (vii) TRF2 density and (viii) percentage of cells in G1, S and G2/M phase. The change of these absolute reference values obtained for the control siRNA is given for each siRNA in percent or percentage points relative to the absolute values (p-value < 0.05, Kolmogorov-Smirnov test or Welch's t-test (for cell cycle analysis), $n \geq 3$). Changes that were not statistically significant are marked by n.s. (= not significant). The table is provided as a separate Excel file.

Download Table S2

Supplementary Table S3. Primers for quantitative real-time PCR.

Target	Sequence (5'->3')
-actin	TCCCTGGAGAAGAGCTACGA
	AGCACTGTGTTGGCGTACAG
CBX3 (HP1)	AAAATGGCCTCCAACAAAAC
	TTCCCATTCACTACACGTCG
HDAC7	CTCACTGTCAGCCCCAGAG
	CTGGTGCTTCAGCATGACC
MRE11A	CAGAAAGAGGGATGGGTGAA
	AACGACGTACCTCCTCATCG
NBS1	GTTGAGTCCAAGAAGCAGCC
	GTTTTCTTTCCTGCCGTCCT
NSBP1 (HMGN5)	TGTGCCAGTTACACCAGAGG
	CAACTGCTTGGGCACTTGT
PARP2	GGCACAAATCAAGGCAGGTTA
	AAGTCATGCGGAATCCTGGTG
RAD50	TTGTGAACAAGGATCTGGATATTTA
	TCGCCACAGGTCACGTATAA
RAP1A	TCTCACTGCACCTTCAATGG
	CTGTCAGAGCAGACTTCCCA
SENP6	AGCGCAGGGGAGATTACTTT
	TGAGCAGATTTGTCCCATCTT
SUV420H2	CATGACTGCAAACCCAACTG
	GCCGTAGAAGCATGTCACCT
TRF2	GTACCCAAAGGCAAGTGGAA
	TGACCCACTCGCTTTCTTCT